

# Can multistate dark matter annihilation explain the high-energy cosmic ray lepton anomalies?

Marco Cirelli<sup>1,2</sup>, James M. Cline<sup>1,3</sup>

<sup>1</sup>*CERN Theory Division, CERN, Case C01600, CH-1211 Genève, Switzerland*

<sup>2</sup>*Institut de Physique Théorique, CNRS URA 2306 & CEA/Saclay, F-91191 Gif-sur-Yvette, France*  
and

<sup>3</sup>*Physics Department, McGill University, 3600 University Street, Montréal, Québec, Canada H3A 2T8*  
e-mail: marco.cirelli@cea.fr, jcline@physics.mcgill.ca

(Dated: 17 May 2010)

Multistate dark matter (DM) models with small mass splittings and couplings to light hidden sector bosons have been proposed as an explanation for the PAMELA/Fermi/H.E.S.S. high-energy lepton excesses. We investigate this proposal over a wide range of DM density profiles, in the framework of concrete models with doublet or triplet dark matter and a hidden SU(2) gauge sector that mixes with standard model hypercharge. The gauge coupling is bounded from below by the DM relic density, and the Sommerfeld enhancement factor is explicitly computable for given values of the DM and gauge boson masses  $M$ ,  $\mu$  and the (largest) dark matter mass splitting  $\delta M_{12}$ . Sommerfeld enhancement is stronger at the galactic center than near the Sun because of the radial dependence of the DM velocity profile, which strengthens the inverse Compton (IC) gamma ray constraints relative to usual assumptions. We find that the PAMELA/Fermi/H.E.S.S. lepton excesses are marginally compatible with the model predictions, and with CMB and Fermi gamma ray constraints, for  $M \cong 800$  GeV,  $\mu \lesssim 200$  MeV, and a dark matter profile with noncuspy Einasto parameters  $\alpha \gtrsim 0.20$ ,  $r_s \sim 30$  kpc. We also find that the annihilating DM must provide only a subdominant ( $\lesssim 0.4$ ) component of the total DM mass density, since otherwise the boost factor due to Sommerfeld enhancement is too large.

PACS numbers: 95.35.+d, 98.70.Sa, 12.60.Cn

## I. INTRODUCTION

Dark matter (DM) annihilating in the galaxy has been proposed as the explanation for a number of current experimental anomalies. The Payload for Antimatter-Matter Exploration and Light-nuclei Astrophysics (PAMELA) experiment has observed an excess in the positron fraction in the energy range 10–100 GeV [1], and the Fermi Large Area Telescope (LAT) [2] observes an excess in  $e^+ + e^-$  at energies up to 1 TeV, compared to the predictions of conventional diffusive models. The High Energy Stereoscopic System (H.E.S.S.) [3], too, observes a steepening in the spectrum around a few TeV which is in agreement with the Fermi-LAT excess. On the other hand, PAMELA does not observe excess antiprotons. Therefore TeV-mass particles that can annihilate preferentially into leptons are the preferred DM candidates for explaining these anomalies [4–8].

Theories of leptophilic annihilating DM have come under increasing pressure from a number of complementary constraints, due to the radio and gamma ray (GR) emissions that should be produced by the annihilation process itself (‘prompt’ gamma rays) [9–12] or by the high energy  $e^\pm$ , via synchrotron radiation in the galactic magnetic field or via inverse Compton scattering on cosmic microwave background (CMB) photons and the galactic radiation field (starlight) [13–20]. Such radiation could also partially reionize the universe after recombination, leading to distortions in the CMB [21–25]. Finally, relevant constraints are imposed by extragalactic gamma

rays, produced by the annihilations in forming DM halos [23, 26, 27]. Many models of annihilating DM are seemingly ruled out by overproducing such radiation. In particular, inverse Compton gamma rays produced in the galaxy would contribute to the GR spectrum observed by Fermi-LAT.

A precise assesment of the strength of Fermi inverse Compton (IC) constraints depends however upon the details of the assumed DM density profile  $\rho(r)$ . The strongest constraints come from close to the Galactic Center (GC); therefore they can be satisfied if  $\rho(r)$  is not strongly peaked as  $r \rightarrow 0$ , where  $r$  is the distance from the GC. Usually such dependence is illustrated by choosing a few different parametrizations of the profile with varying cuspieness (*e.g.*, the peaked Navarro-Frenk-White profile [28] as opposed to the cored isothermal [29] or Burkert profiles [30]).  $N$ -body simulations and observations of our own galaxy suggest a reasonable range of shapes for  $\rho(r)$ , and it would be interesting to explore the dependence of the constraints on the characteristics of  $\rho(r)$  within such a range. One purpose of the present work is to fill this gap by quantifying the strength of the IC constraint for a wide range of DM density profiles. We limit ourselves to the Einasto parametrization [31, 32], which we find to be useful for this purpose since it allows for continuous variation in the cuspieness and it has been used to fit the results of high-resolution  $N$ -body simulations.

The constraints also depend upon which leptons, and how many of them, are assumed to be produced in the

DM annihilations. For example, models that produce only  $e^+e^-$  are more strongly constrained, for a given DM mass  $M$ , than those that produce two  $e^\pm$  pairs, since the spectrum of the former is harder. This is a relevant distinction since some of the models that are most natural from the particle physics point of view necessarily produce the  $4e$  (or at least  $2e$  plus an invisible hidden sector gauge boson) rather than the  $2e$  final state. Likewise models that produce muons are more strongly constrained than those that produce only electrons. Moreover models using the gauge kinetic mixing portal produce an admixture of  $e^\pm$ ,  $\mu^\pm$  and  $\pi^\pm$  rather than just a single kind of final state. Failing to recognize these distinctions, one could be misled into thinking that the general class of models is excluded, even though there may exist specific examples that satisfy all the constraints.

Thus another goal of the present work is to explore in detail the viability of a very specific set of annihilating DM models, which are also theoretically motivated [33]–[36]. Namely we consider DM  $\chi_i$  transforming under a nonabelian hidden sector gauge symmetry, taking the simplest example of  $SU(2)$  and the lowest representations (doublet or triplet) for the DM. One of the dark gauge bosons  $B_i$  is assumed to mix with standard model hypercharge (and thus the photon) through a dimension-5 gauge kinetic mixing operator. This model has a number of appealing features. The DM annihilates into dark gauge bosons,  $\chi\chi \rightarrow BB$ . By assuming the gauge symmetry breaks below the GeV scale, so the  $B_i$ 's have mass  $\mu \lesssim 1$  GeV, it is assured that only light leptons or  $\pi^\pm$  are produced by the gauge boson decays, and no antiprotons that would be in conflict with the PAMELA observations. The annihilation cross section is naturally enhanced by Sommerfeld effect [33, 37] in this model, allowing it to have the correct relic density in the Early Universe, even though the cross section in the galaxy must be larger by a factor of order 100 than that needed for thermal freeze-out.

A distinctive feature of the model is that small mass splittings  $\delta M \sim 1$  MeV between the DM states are generated at one loop. Such splittings can be important for making the model consistent with direct detection constraints, by causing DM scattering on nucleons to be inelastic and endothermic. This allows the rate of DM interactions in detectors to be sufficiently suppressed despite having relatively large couplings to nucleons [33]. The mass splittings can moreover lead to a significant increase in the Sommerfeld enhancement factor [38], which effect we take into account here. In addition, they can potentially help to explain the annual modulation observed by DAMA/LIBRA through the inelastic DM mechanism (see for example [39]), or the 511 keV excess observed by INTEGRAL [40] using the excited DM mechanism [41]–[44], although we do not explore these directions in the present work.

A further refinement we make compared to most previous analyses is to take into account the dependence of the Sommerfeld enhancement on the position in the

Galaxy, an effect that was first pointed out in ref. [45]. The Sommerfeld enhancement depends sensitively on the DM velocity, and both the DM velocity dispersion and escape velocity depend upon  $r$ . We find that this typically makes the enhancement larger near the galactic center where the gamma rays that are most important for the IC constraint are produced. The constraint thus becomes harder to satisfy than in models with a spatially constant boost factor, as is usually assumed.

Nevertheless, we find examples of models that are marginally able to produce leptons consistent with the PAMELA and Fermi observations, and which are also barely consistent with the various gamma ray constraints. The preferred models have DM with  $M \cong 800$  GeV and gauge boson masses below 200 MeV, so that only electrons and no muons or charged pions are produced in the annihilations. However we find that the Sommerfeld enhancement factor would always be *too large* to achieve this concordance if the DM was present at the expected relic density. We are obliged to suppress the rate of annihilations by introducing a factor  $1/f$  in the density of the annihilating component. This can be achieved by increasing the gauge coupling appropriately so that the relic density is reduced. The minimum reduction  $1/f = 0.4$  occurs if the DM mass splitting is negligible, and smaller values  $1/f \cong 0.14 - 0.2$  are needed if  $\delta M \sim 1$  MeV. This comes about because of the  $\delta M$ -dependence of the Sommerfeld enhancement factor for multistate DM annihilations [38].

In the present work we do not consider astrophysical boost factors due to increased annihilation rate in substructures of the main halo [46]–[52]. Inclusion of these effects would presumably strengthen the gamma ray constraints on the models, but on the other hand a fully consistent treatment of substructure effects should simultaneously consider the modification to the lepton signal from annihilations in subhalos [53]. This could conceivably have a compensating effect that would weaken the constraints due to requiring less  $e^\pm$  production near the galactic center [54]. Further investigation of this issue is in progress.

We start by introducing the particle physics models in section II, and recalling the constraint upon the dark  $SU(2)$  gauge coupling imposed by the relic density. In section III we analyze how large an enhancement factor is needed for the models to explain the anomalous lepton observations, the theoretical computation of the Sommerfeld enhancement, and its phase space average in the galaxy. Section IV explains how we implement the inverse Compton  $\gamma$  ray constraint for general DM Einasto profiles, while other relevant constraints are discussed in section V. Our main results showing which parameter ranges can be compatible with all the observations are presented in section VI. We discuss their implications in section VII. Three appendices give details for the branching ratio of ground state DM annihilation into leptons (app. A), the multistate Sommerfeld enhancement (app. B) and the calculation of the DM escape velocity (app.

C) as a function of radial position.

## II. PARTICLE PHYSICS MODELS

### A. The models

For the purpose of testing a concrete and specific model, we will analyze the simplest examples of non-abelian hidden sector models that can explain the various cosmic ray anomalies; namely a dark SU(2) gauge group under which the DM transforms as a doublet or a triplet [35, 36]. The Lagrangian for the DM and the gauge bosons is

$$\mathcal{L} = \frac{1}{2} \bar{\chi}_i (i \not{D}_{ij} - M_\chi \delta_{ij}) \chi_j - \frac{1}{4g^2} B_{\mu\nu}^a B_a^{\mu\nu} - \frac{1}{\Lambda} \Delta_a B_a^{\mu\nu} Y_{\mu\nu} \quad (1)$$

We assume that the dark Higgs triplet  $\Delta_a$  gets a VEV in the  $a = 2$  direction, so that  $B_2$  mixes with the standard model hypercharge  $Y_{\mu\nu}$  with strength

$$\epsilon = \langle \Delta_2 \rangle / \Lambda \quad (2)$$

This causes  $B_2$  to acquire a coupling of strength  $\epsilon q$  to any SM particle of charge  $q$ , and therefore to mediate the decay  $\chi_2 \rightarrow \chi_1 e^+ e^-$  in the doublet model, or  $\chi_3 \rightarrow \chi_1 e^+ e^-$  in the triplet model.<sup>1</sup> The value of  $\epsilon$  is not strongly constrained; it can be anywhere between  $10^{-2}$  and  $10^{-9}$  [36] (except for a small region around  $10^{-6}$ - $10^{-7}$  excluded by the E137 experiment if the dark gauge boson mass is less than 400 MeV [55]).

These models can explain the PAMELA positron excess and Fermi/LAT  $e^\pm$  excess through the annihilation  $\chi_1 \chi_1 \rightarrow B_2 B_2$ , followed by the decays  $B_2 \rightarrow \bar{f} f$ , where  $f$  is any charged SM particle with mass less than  $\mu_2/2$  (where  $\mu_2$  denotes the mass of  $B_2$ ). Although higher mass fermions can be produced through off-shell gauge bosons, such processes have a much smaller cross section than those in which the  $B_2$ 's are on shell. Using this fact, one can account for the lack of any antiproton excess in the PAMELA observations by assuming that  $\mu_2$  is less than  $2m_p$ .

### B. Relic density

Ref. [36] computed the cross section for  $\chi\chi \rightarrow BB$  and determined that it leads to the right relic density from thermal freezeout in the doublet or triplet model, if the gauge coupling  $\alpha_g = g^2/4\pi$  has strength

$$\alpha_g = \left( \frac{M}{1 \text{ TeV}} \right) \times \begin{cases} 0.077, & \text{doublet} \\ 0.031, & \text{triplet} \end{cases} \quad (3)$$

<sup>1</sup> The gauge couplings have the form  $g \bar{\chi}_i \sigma_{ij}^a \not{B}_a \chi_j$  or  $\frac{1}{2} g \epsilon_{abc} \bar{\chi}_a \not{B}_b \chi_c$  respectively, in the doublet and triplet models.

corresponding to  $g = 0.98, 0.62$  respectively at  $M = 1$  TeV. We will adopt this relation between  $g$  and  $M$  in our analysis of the triplet model. For the doublet model, the DM must be Dirac in order to have a bare  $M \bar{\chi} \chi$  mass term that respects the SU(2) gauge symmetry. It could therefore have a chemical potential that fixes its relic density independently of its annihilation cross section. This could provide motivation to consider  $\alpha_g$  as an additional free parameter for the doublet model, if one can find a mechanism for producing the asymmetry between  $\chi$  and  $\bar{\chi}$ .

In later sections we will find that it is difficult to satisfy all constraints if the annihilating DM has the full allowed relic density, because the Sommerfeld enhancement of the annihilation cross section is too large. A more general possibility is that the gauge coupling exceeds (3) by a factor  $\sqrt{f}$ , which leads to an enhancement in the cross section  $\sigma \rightarrow f\sigma$ , and a consequent suppression in the density by  $\rho \rightarrow \rho/f$ . Since the signals scale like  $\rho^2 \sigma$ , this leads to a reduction by  $1/f$  in the rate of annihilations in the galaxy. Thus more generally we will consider gauge couplings given by

$$\alpha_g = \sqrt{f} \left( \frac{M}{1 \text{ TeV}} \right) \times \begin{cases} 0.077, & \text{doublet} \\ 0.031, & \text{triplet} \end{cases} \quad (4)$$

where  $f \geq 1$ .

If  $f > 2$ , then less than half of the DM resides in the ground state, and there must exist some additional DM sector to make up the rest of the mass density. If  $1 < f < 2$ , the needed reduction could happen naturally within the model due to the fact that some fraction (less than 1/2) of the DM resides in one of the excited states, assuming it is stable, and that it is not able to annihilate into leptons. (Our triplet DM model provides such an example.) A quantitative calculation of the relic density of the excited state is beyond the scope of this paper, but will be carried out in ref. [44].

### C. Higgs sector

The model must also include a dark Higgs sector to break the SU(2) gauge symmetry and give masses  $\mu \lesssim 1$  GeV to the gauge bosons. One-loop self-energy corrections to the DM masses induce mass splittings of order  $\delta M \sim \alpha_g \delta \mu$  if the gauge boson masses themselves are split by an amount of order  $\delta \mu$ . The splittings  $\delta M \sim 1$  MeV are potentially useful for explaining the INTEGRAL 511 keV gamma rays by the excited dark matter mechanism, and they are needed to satisfy constraints from direct detection unless the mixing parameter  $\epsilon$  defined in (2) is small,  $\epsilon < 10^{-6}$  [33]. Larger mixing  $\epsilon \sim 10^{-3}$  are more interesting from the perspective of laboratory tests by fixed-target experiments.

In the simplest and most predictive models, the DM states would have no Yukawa couplings to Higgs bosons

of the hidden sector.<sup>2</sup> If one is also interested in trying to address the 511 keV gamma ray excess, the relation  $\delta M = \frac{1}{2}\alpha_g\delta\mu$  gives a constraint on splittings between the gauge boson masses. The DM mass splittings should not be much more than of order 1 MeV; otherwise excited DM decays would produce  $e^\pm$  of too high energy to be compatible with the narrow observed 511 keV spectrum. For the triplet DM model with  $\alpha_g = 0.031$  for  $M = 1$  TeV, we thus expect that  $\delta\mu \lesssim 180$  MeV if the largest DM mass splitting is  $\delta M = 3$  MeV. Moreover we will show that models with  $\mu \sim 200$  MeV can more easily satisfy stringent  $\gamma$  ray constraints.

#### D. Explicit example

Ref. [36] showed that the minimal Higgs sector for splitting triplet DM is one that gives a VEV to an additional triplet Higgs field  $\Delta'_a$  in a direction orthogonal to that of the first triplet VEV, *e.g.*,  $\Delta'_1$ . We do not wish to commit ourselves to a particular Higgs potential in the present analysis. Instead, we will assume that it is possible to design one that gives the desired DM mass splittings of order 100 keV to a few MeV, and gauge boson masses of order a few 100 MeV. In fact, this is quite reasonable even in the context of the simplest model with two Higgs triplets. Using the analysis of ref. [36], the mass splittings  $\delta M_{13} = 3.1$  MeV,  $\delta M_{23} = 100$  keV and gauge coupling  $g = 0.62$  imply that  $\Delta'_1 = 320$  MeV,  $\Delta'_2 = 80$  MeV, and the gauge boson masses are  $\mu_1 \cong 50$  MeV,  $\mu_2 \cong \mu_3 \cong 200$  MeV using this simplest Higgs sector.

### III. SOMMERFELD ENHANCEMENT FOR PAMELA/FERMI LEPTON SIGNALS

In this section we explain how we calculate the effective cross section for annihilating DM to produce high-energy  $e^\pm$  (and possibly heavier charged particles) in the galaxy, relevant for explaining the PAMELA and Fermi  $e^\pm$  excesses. A particularly simple case to focus upon is that where the mass  $\mu$  of the  $B_2$  gauge boson is below the threshold for producing a  $\mu^+\mu^-$  pair. In that case one need only consider final states consisting of  $e^\pm$ . Moreover the cross section to fit the PAMELA/Fermi lepton data is smaller in this case, and thus easier to achieve from the model-building perspective. Another reason for preferring the  $4e$  channel is that it is not ruled out by CMB reionization constraints, whereas the  $4\mu$  channel is (depending upon the assumed value of the local DM density  $\rho_\odot$ , as we will discuss); this is apparent in figure 1.

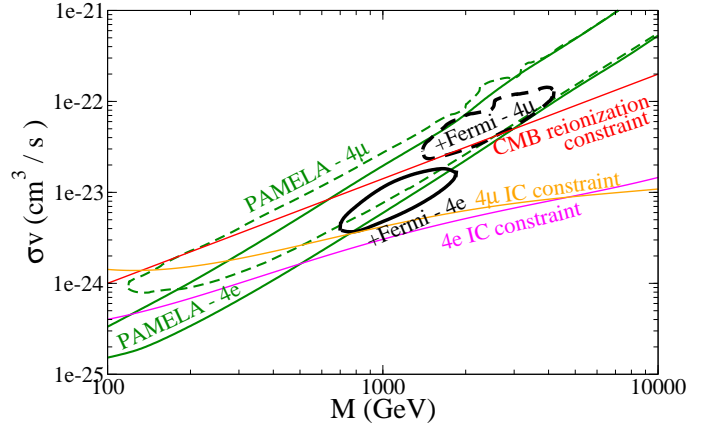


FIG. 1: Heavy lines: allowed regions for explaining the PAMELA and Fermi lepton excesses, assuming  $4e$  or  $4\mu$  final states, from ref. [17]. The fits assume an Einasto DM profile with  $\rho_\odot = 0.3$  GeV/cm<sup>3</sup>,  $\alpha = 0.17$  and  $r_s = 20$  kpc. Narrow lines show constraints from CMB [24] and inverse Compton gamma rays [17].

#### A. Cross section ratio for $\chi_1\chi_1 \rightarrow e^\pm$

Although the models we consider could have an excited DM state that is stable or metastable, the ground state normally should have a larger density  $n_1$  due to downscattering processes like  $\chi_2\chi_2 \rightarrow \chi_1\chi_1$  in the early universe. To simplify the analysis, we assume that it is a good approximation to ignore annihilations involving the subdominant component for the production of leptons via  $\chi\chi \rightarrow 4e$ . For the triplet DM model, there are in fact no such annihilations in the form  $\chi_2\chi_2 \rightarrow 4e$  because  $\chi_2$  does not couple to  $B_2$ , the gauge boson that we have assumed to be the only one mixing with the SM. The only annihilations we miss in this case are of the form  $\chi_1\chi_2 \rightarrow B_1 e^+ e^-$ , where the  $B_1$  appears as missing energy.

It is potentially important to realize that only the ground state (and possibly some small addition of excited state particles) contribute to the annihilation in the galaxy, because the cross section for  $\chi_i\chi_j$  to annihilate is different from that for  $\chi_i\chi_j$  in the early universe. They are related by the ratio  $b_{11}$ ,

$$\sigma(\chi_1\chi_1 \rightarrow e^\pm) = b_{11}\sigma(\chi_i\chi_j \rightarrow \text{any}) \quad (5)$$

which in the doublet and triplet models is given by

$$b_{11} = \begin{cases} \frac{5}{9}, & \text{doublet} \\ \frac{8}{7}, & \text{triplet} \end{cases} \quad (6)$$

as we explain in appendix A.<sup>3</sup>

<sup>2</sup> In a model with only triplet Higgses and Majorana DM, the only potentially gauge invariant coupling  $\epsilon_{abc}\chi_a\chi_b\Delta_c$  in fact vanishes.

<sup>3</sup> we thank Tracy Slatyer for pointing out an error in our original

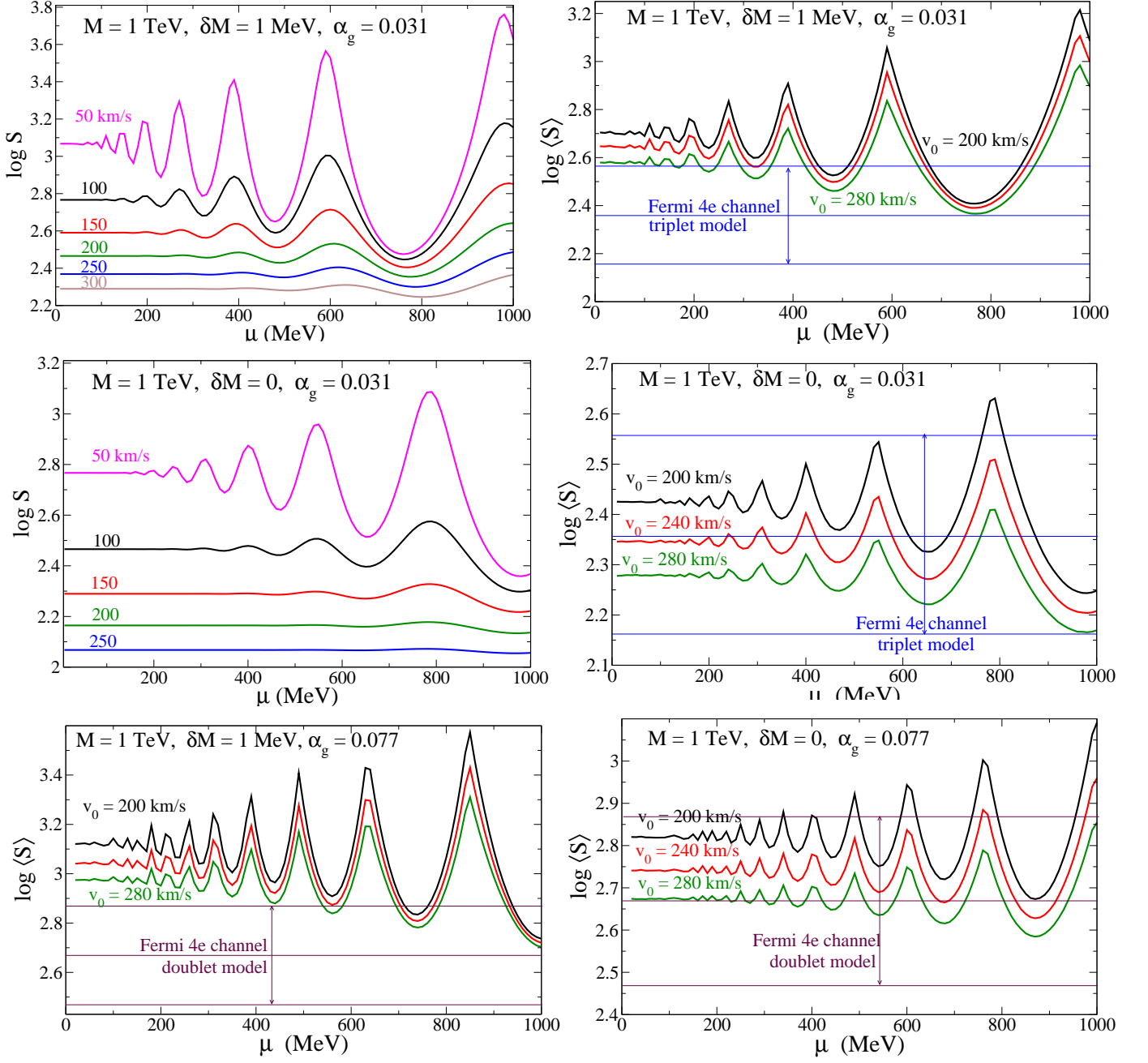


FIG. 2: Upper left: Sommerfeld enhancement factor (B1) as a function of gauge boson mass  $\mu$  for DM mass  $M = 1$  TeV, mass splitting  $\delta M = 1$  MeV, and gauge coupling  $\alpha_g = 0.031$ . Different curves are labeled by DM velocity in center of mass frame, in km/s. Upper right: the same, but averaged over the DM velocity distribution functions as in (10), for three different circular velocities  $v_0 = 200, 240$  and  $280$  km/s. The allowed regions for Fermi with  $4e$  annihilation channel for the doublet and triplet DM models, assuming solar density  $\rho_\odot = 0.3$  GeV/cm<sup>3</sup> and DM fraction  $f = 1$  (see eq. (4)) are shown by horizontal lines. Central panels: same as upper but with vanishing mass splitting  $\delta M = 0$ . Lower panels: velocity-averaged Sommerfeld enhancement factors versus  $\mu$  for doublet model, with  $\alpha_g = 0.077$  and  $\delta M = 1$  MeV (left),  $\delta M = 0$  (right).

## B. Sommerfeld enhancement for multistate DM

The boost factor needed for explaining the PAMELA/Fermi  $e^\pm$  observations can be inferred using figure 1, which shows the  $3\sigma$ -allowed regions for  $M$  and  $\sigma v$ , assuming  $4e$  and  $4\mu$  final states, and

computation of this quantity

also assuming the solar neighborhood DM density to be  $\rho_\odot = 0.3 \text{ GeV/cm}^3$ . The central value of the  $4e$  allowed region has  $\sigma v = 10^{-23.1 \pm 0.2} \text{ cm}^3/\text{s}$  at  $M \cong 1.1 \text{ TeV}$ , while the  $\sigma v$  needed for the right relic abundance is  $3 \times 10^{-26} \text{ cm}^3/\text{s}$ . This leads to a required boost factor of  $B = 10^{-23.1 \pm 0.2}/(b_{11} \cdot 3 \times 10^{-26})$ . Allowing for  $\sigma v \rightarrow f \sigma v$  and  $\rho \rightarrow \rho/f$  as described in section II B, the required boost factor scales as  $B \rightarrow fB$ . For the doublet and triplet models, using the gauge couplings (4), this gives

$$\log B_{4e} = \log f + \begin{cases} 2.67 \pm 0.2, & \text{doublet} \\ 2.36 \pm 0.2, & \text{triplet} \end{cases} \quad (7)$$

for the boost factor needed in the  $4e$  annihilation channel.

To get a feeling for the ability of the models to achieve large enough boosts, we start by computing the Sommerfeld enhancement factor for a fixed DM mass of  $M = 1 \text{ TeV}$  near the central region allowed by Fermi with  $4e$  final states. For this purpose one should take into account that there is more than one DM state, so the usual Sommerfeld factor for single-state DM is not appropriate. The general case has not been solved explicitly, but that of two states with therefore a single mass splitting was recently analyzed in [38], where it was found that the enhancement factor can be approximated by eq. (B1) given in appendix B.

The result (B1) applies directly to the doublet model, where there are only two states, but only approximately in the case of the triplet model, since the latter has three states and two mass splittings. Since the enhancement is an increasing function of  $\delta M$ , one might reasonably expect the multistate effect in the triplet model to be captured by choosing the largest of the two mass splittings. We make this assumption, which in a more ambitious study should be checked. It is however a technically challenging problem.

### C. Velocity-averaged enhancement at $r = r_\odot$

We must compute the boost factor in the neighborhood of the Sun in order to predict the rate of high-energy lepton production from DM annihilations. The Sommerfeld enhancement depends upon the relative velocity of the DM particles, which is usually characterized by a Maxwellian distribution

$$f(v) = N e^{-v^2/v_0^2} \theta(v - v_{\text{esc}}) \quad (8)$$

with a cutoff for  $v$  above some escape velocity  $v_{\text{esc}}$ . The value  $v_0$  is commonly taken to be  $220 \text{ km/s}$  at the solar radius  $r_\odot = 8.3 \text{ kpc}$ , although higher values  $\sim 250 \text{ km/s}$  have been advocated more recently [56]. The range  $v_0 \in 200 - 280 \text{ km/s}$  is suggested by the compilation of different measurements in ref. [57]. The escape velocity is directly correlated with  $v_0$ , as detailed in appendix C. There we motivate our choice for the  $r$ -dependent relation

$$v_{\text{esc}}^2(r) = 2v_0^2(r) [2.39 + \ln(10 \text{ kpc}/r)] \quad (9)$$

in the region  $r < 10 \text{ kpc}$ . (We elaborate on the  $r$  dependence of  $v_0$  in section VI A.) At the solar radius, which we take to be  $r_\odot = 8.33 \text{ kpc}$  [58], this gives  $v_{\text{esc}} = 2.53 v_0$ , corresponding to escape velocities in the range  $440 - 610 \text{ km/s}$ . This is in reasonable agreement with constraints from direct measurements of high-velocity stars [59]. We need to average  $S(|\vec{v}_1 - \vec{v}_2|)$  over the phase space,

$$\langle S \rangle = \int d^3v_1 d^3v_2 f(v_1) f(v_2) S(|\vec{v}_1 - \vec{v}_2|) \quad (10)$$

### D. Predicted versus desired enhancement factor values

In figure 2 the dependence of the Sommerfeld enhancement  $S$  and its velocity average  $\langle S \rangle$  on the gauge boson mass  $\mu$  is shown, for the example of  $M = 1 \text{ TeV}$  and for the triplet model with  $\alpha_g = 0.031$ , as well as the doublet with  $\alpha_g = 0.077$ . These are the gauge couplings needed for the right relic density in the respective cases. The extra enhancement due to the mass splitting  $\delta M = 1 \text{ MeV}$  is quite significant; in fact it tends to give rise to boost factors that are too large compared to the values needed to explain the high-energy lepton excesses. The effect of  $\delta M$  actually saturates around  $\delta M = 600 \text{ keV}$  for the triplet model and  $\delta M = 100 \text{ keV}$  for the doublet model; the enhancement remains roughly constant for larger values (however the validity of the approximations leading to (B1) breaks down if  $\delta M \gtrsim \alpha_g^2 M$ ).

We conclude that, from the point of view getting the right boost factor, there is no need for the mass splitting, and in fact too large a mass splitting is disfavored. However this can be compensated by invoking the  $f$ -factor of section II B, since taking  $f > 1$  increases the value of the needed boost factor.

## IV. INVERSE COMPTON GAMMA RAY CONSTRAINT

To undertake a thorough exploration of the parameter space, we must take into account constraints that could rule out the models. The interpretation of the PAMELA and Fermi excesses as being due to DM annihilation has come under pressure from a number of complementary constraints. Many of these arise from radiation that would be produced by the leptons after annihilation, which should be directly detectable as gamma rays or radio emission in the galaxy, or indirectly in distortions of the cosmic microwave background by contributing to the reionization of the early universe. The most stringent constraint on our model is from inverse Compton scattering in the galaxy. We therefore consider it separately in this section, and discuss other constraints in section V.

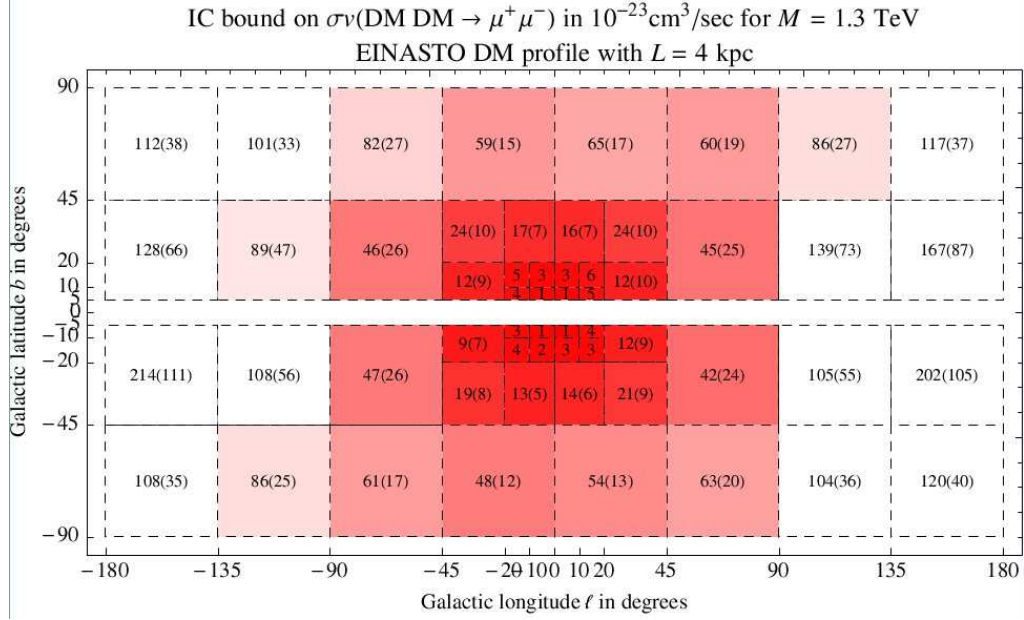


FIG. 3: Regions near galactic center used by ref. [17] for computing the Fermi IC bound. Numbers in each region refer to constraints arising for a particular annihilation channel (into  $\mu^+\mu^-$ ), but size and shape of regions are the same for the channel we consider,  $2e^+2e^-$ . Courtesy of A. Strumia.

#### A. Characterization of the bound

If DM annihilates into charged particles, the latter will undergo inverse Compton scattering on the galactic radiation field (for example, starlight) to produce high energy gamma rays that could be detected by the Fermi LAT. Several authors have considered the constraints arising from the nondetection of such a signal [13–20]. Most of these assume a two-lepton final state rather than four leptons, as is the case in our models. The constraints on the former are stronger because their spectrum is harder than in the four-body case. Ref. [17] has considered four-lepton final states for several DM density profiles, so we adopt their results for the present analysis.

The resulting fits of [17] for the PAMELA/Fermi excesses and the IC constraints for the  $4e$  and  $4\mu$  channels are shown in figure 1, for a particular choice of Einasto profile,

$$\rho(r) = \rho_\odot \exp \left[ -\frac{2}{\alpha} \left( \left( \frac{r}{r_s} \right)^\alpha - \left( \frac{r_\odot}{r_s} \right)^\alpha \right) \right] \quad (11)$$

with  $\rho_\odot = 0.3 \text{ GeV/cm}^3$ ,  $\alpha = 0.17$ ,  $r_s = 20 \text{ kpc}$ , and  $r_\odot = 8.5 \text{ kpc}$ . The maximum allowed annihilation cross

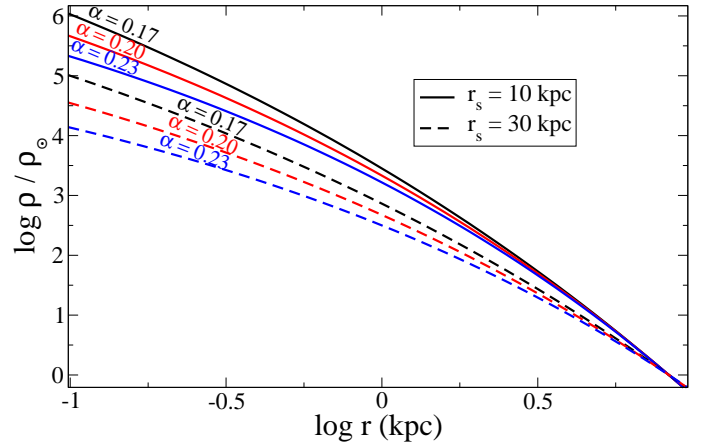


FIG. 4: Einasto density profiles normalized to  $\rho_\odot$  for  $\alpha = 0.17, 0.20, 0.23$  and  $r_s = 10 \text{ kpc}$  (solid curves) or  $r_s = 30 \text{ kpc}$  (dashed curves)

section for these two cases can be approximated as<sup>4</sup>

$$\begin{aligned} 4e : \log \sigma_{4e} v &= -15.14 - 14.66 x + 8.00 x^2 - 1.78 x^3 \\ &\quad + 0.144 x^4 \\ 4\mu : \log \sigma_{4\mu} v &= -8.245 - 21.37 x + 10.43 x^2 - 2.136 x^3 \\ &\quad + 0.161 x^4 \end{aligned} \quad (12)$$

where  $\sigma v$  is in units of  $\text{cm}^3/\text{s}$  and  $x = \log M$  with  $M$

<sup>4</sup> tables on which these fits are based provided by A. Strumia



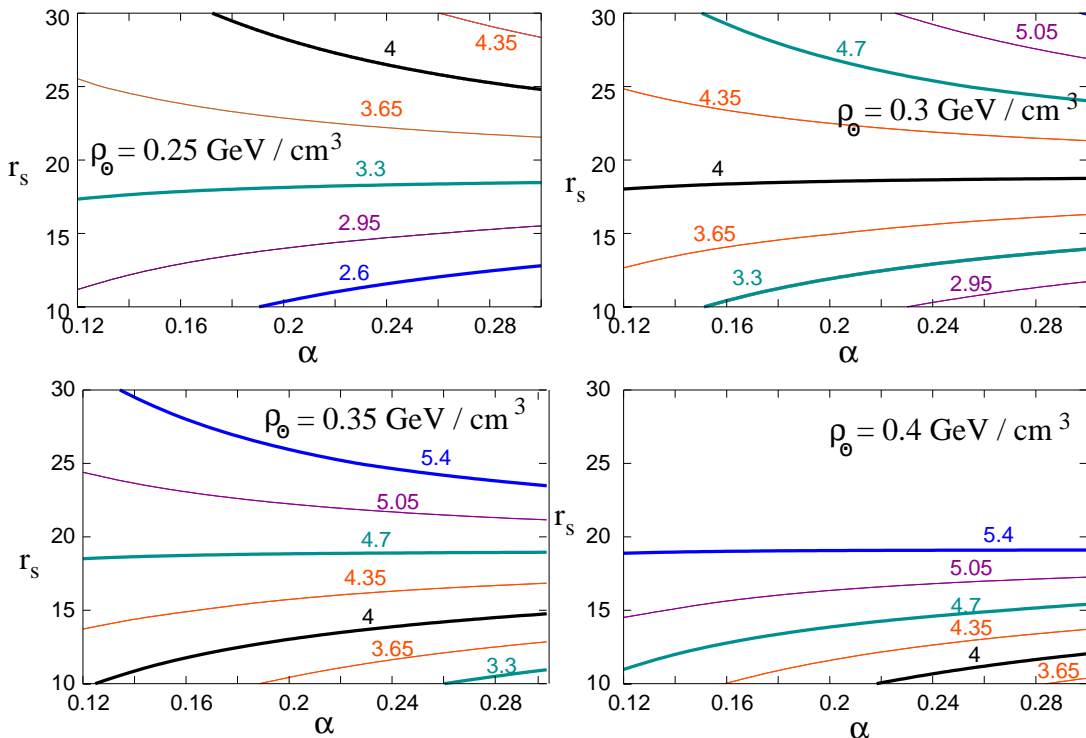


FIG. 5: Contours of  $M_{60}/(10^{11} M_{\odot})$  ( $M_{60}$  being the mass contained within 60 kpc) in the plane of  $\alpha$  and  $r_s$  (in kpc units), for several values of  $\rho_{\odot}$ . The heavy line labeled “4” is the central value, and other heavy lines (at  $4 \pm 0.7$  and  $4 \pm 1.4$ ) denote the neighboring  $1\sigma$  and  $2\sigma$  confidence intervals determined by ref. [70].

in GeV. The constraints are found by comparing the observed gamma ray spectrum from Fermi data with the predicted IC contribution from the DM-produced leptons, and demanding that the latter do not exceed the former in any energy bins by more than  $3\sigma$ . Ref. [17] carried out this procedure for different regions of the sky, similar to those depicted in fig. 3. The regions closest to the galactic center are the ones that give the strongest constraint on the cross section, resulting in the bounds (12). It is worthwhile to notice that the inner  $5^\circ$  of galactic latitude have not been used in deriving the constraints, due to the difficulties of interpreting foregrounds associated with the disk of the galaxy. We have adopted ref. [17]’s constraints relative to the ‘MED’ propagation model for  $e^\pm$ , corresponding to a diffusion zone thickness of  $L = 4$  kpc; the results from other choices (except for the extreme value  $L = 1$  kpc) are not significantly different in the range of DM masses in which we are interested.

For realistic models of the type we consider, if the gauge boson is heavy enough to decay into muons, then electrons will also necessarily be produced with some nonnegligible probability, depending only on the relative phase spaces for decays into the two different final states. Moreover charged pions will also be produced if the gauge boson mass  $\mu$  is greater than  $2m_\pi$ . In such cases the actual bound will be somewhere in between  $\sigma_{4e}$  and  $\sigma_{4\mu}$  given in (12). We will avoid the uncertainty of how to correctly interpolate between the two bounds by restrict-

ing our attention to the case  $\mu < 2m_\mu$ , so that only the  $4e$  bound applies.

## B. Dependence of IC bound on DM profile

Figure 1 shows that for the assumed fiducial density profile (11), the constraints rule out the Fermi-allowed regions. This can be circumvented however by considering DM density profiles that are less strongly peaked near the galactic center, where the most stringent constraints come from. With the Einasto profile, both  $\alpha$  and  $r_s$  have an effect on the cusiness of  $\rho(r)$  near the galactic center, which is illustrated in figure 4; larger values of  $\alpha$  or  $r_s$  weaken the bound. One of our goals is to quantify this statement to determine the range of  $\alpha$  and  $r_s$  that gives a consistent description of the PAMELA/Fermi anomalies in terms of DM annihilation.

### 1. Theoretical and observational constraints on the DM profile

Let us first consider what are the reasonable ranges of variation for the halo profile parameters  $\alpha$  and  $r_s$  based on theoretical and observational considerations.  $N$ -body simulations like Aquarius find  $0.115 < \alpha < 0.179$  [32]; in a different fit of the same galaxies over a slightly smaller



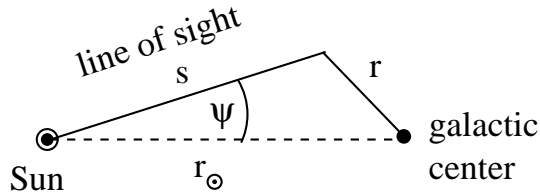


FIG. 6: Representation of the quantities  $r$ ,  $s$ ,  $\psi$  used to compute the  $\bar{J}$  factor (14). The coordinate  $s$  runs along the line of sight in the direction specified by the angle  $\psi$  and is related to  $r$  by  $r(s, \psi) = \sqrt{r_\odot^2 + s^2 - 2r_\odot s \cos \psi}$ .

radial region, ref. [60] finds  $\alpha$  as large as 0.19. These values are for pure DM simulations without baryons; the inclusion of baryons tends to reduce  $\alpha$  dramatically to the range 0.07 – 0.015 due to the concentrating effect of the baryons on the inner halo [60–62]. In contrast, the pure DM simulations find a larger range of  $r_s$ , from 15 kpc to 29 kpc (where we have assumed  $h = 0.7$  for the Hubble parameter, since the results are quoted in units of kpc/ $h$ ). This range also gets decreased when baryons are included, to 5 – 15 kpc. There thus appears to be a conflict between the DM simulations with baryons (BDM) and the annihilating DM interpretation of PAMELA/Fermi events, since the adoption of  $\alpha = 0.15$  and  $r_s = 15$  kpc will only make the IC constraint stronger, compared to values that already rule out the model. We also note that one of the highest resolution simulations, GALO [65], obtains  $\alpha = 0.155$  even without including baryons.

For the allowed range of the solar neighborhood density  $\rho_\odot$ , observations provide tighter constraints than do simulations. The value  $\rho_{\odot,0} \equiv 0.3$  GeV/cm<sup>3</sup> has for a long time been considered standard [66]. More recently a higher central value  $0.385 \pm 0.027$  GeV/cm<sup>3</sup> has been advocated in [67] and  $0.43 \pm 0.15$  GeV/cm<sup>3</sup> has been determined using a method that does not rely upon the detailed form of  $\rho(r)$  in [68].

Observational limits on the ranges of the other Einasto parameters tend to be weaker than the ranges suggested by simulations, but this depends upon the assumed value of  $\rho_\odot$ . One constraint comes from the mass within a given radius inferred from rotation curves of the Milky Way galaxy. Ref. [69] inferred a total mass within 50 kpc of the galactic center,  $M_{50} = 5.3 \times 10^{11} M_\odot$ . More recently, using data from the Sloan Digital Sky Survey, ref. [70] obtained the mass within 60 kpc as  $M_{60} = (4 \pm 0.7) \times 10^{11} M_\odot$ . In fig. 5 we plot contours of  $M_{60}/(10^{11} M_\odot)$  in the  $\alpha$ - $r_s$  plane, for several values of  $\rho_\odot$ . At  $\rho_\odot = 0.4$  GeV/cm<sup>3</sup>, values of  $r_s$  exceeding 20 kpc are disfavored by this measurement, while at  $\rho_\odot = 0.3$  GeV/cm<sup>3</sup> it imposes essentially no constraint.

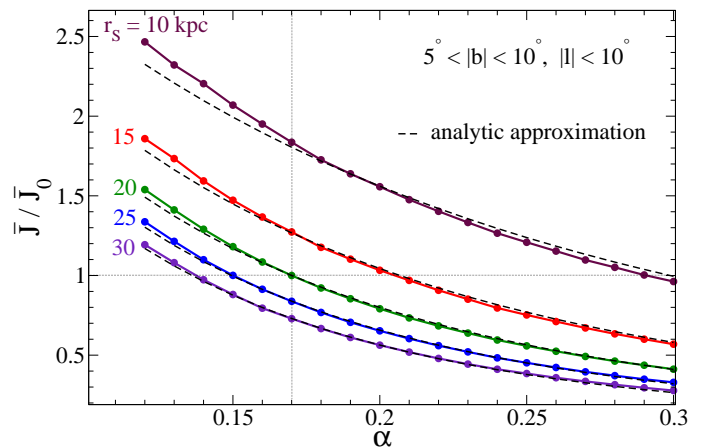


FIG. 7:  $\bar{J}$  factor eq. (14) over the fiducial value used by ref. [17] as a function of  $\alpha$ , for several values of  $r_s$ . Dashed curves are the analytic approximation (15).

## 2. $\bar{J}$ factors for different density profiles

A principal goal of this work is to investigate the sensitivity of the IC bounds in (12) to different choices of the Einasto profile parameters. The dependence upon  $\rho_\odot$  is easy to quantify, since the rate of DM annihilations is proportional to  $\rho^2 \sigma$ . This implies that for a general value of  $\rho_\odot$ , and the fraction  $1/f$  of annihilating DM defined through (4), the upper bound on the annihilation cross section scales as

$$\sigma_{4e} \rightarrow \sigma_{4e} \left( \frac{\rho_{\odot,0}}{\rho_\odot} \right)^2 f^2 \quad (13)$$

relative to that at the reference solar density  $\rho_{\odot,0} = 0.3$  GeV/cm<sup>3</sup> and  $f = 1$ . This means that the constraints become more severe by a factor of  $(0.43/0.3)^2 = 2$  if we adopt the new central value 0.43 GeV/cm<sup>3</sup> of ref. [68] instead of the value 0.3 GeV/cm<sup>3</sup> assumed in ref. [17]. However one must remember that the cross section required to fit the PAMELA and Fermi leptons goes down by the same factor, so in fact the value of  $\rho_\odot$  has little direct effect on the ability of a model to satisfy the IC constraint.<sup>5</sup>

The effect of changing the shape of the profile, on the other hand, is harder to quantify. The correct procedure would require solving the diffusion equation for electrons in the galaxy again for each choice of  $\alpha$  and  $r_s$ , and then recomputing the spectrum of IC scattering. Here we content ourselves with a simpler method of estimation, in which we ignore the changes to the electron diffusion induced by changes in the shape of the profile. In this approximation, the rate of IC scattering due to leptons

<sup>5</sup> Indirectly it has an effect through the constraint from  $M_{60}$ , which makes large values of  $r_s$  hard to achieve when  $\rho_\odot$  is large.

originating from the DM annihilations changes only by a geometrical factor, the averaged  $\bar{J}$  factor, defined as

$$\bar{J} = \frac{1}{\Delta\Omega} \int d\Omega \int_{\text{l.o.s.}} \frac{ds}{r_\odot} \left( \frac{\rho(r(s, \psi))}{\rho_\odot} \right)^2 \quad (14)$$

where the integral along the line of sight is then averaged in  $\psi$  (defined in fig. 6) over the solid angular regions  $\Delta\Omega$  that are used to compute the gamma ray constraints, as shown in fig. 3. As noted above, the relevant regions for obtaining the strongest bound are those with latitude  $5^\circ < |b| < 10^\circ$  and longitude  $|l| < 10^\circ$ . The direction  $\psi$  corresponds to latitude  $b$  and longitude  $\ell$  as  $\cos \psi = \cos b \cos \ell$ .

The resulting  $\bar{J}$  factors, divided by the fiducial one  $\bar{J}_0$  corresponding to the parameters chosen by ref. [17], are shown as a function of  $\alpha$  for several values of  $r_s$  in fig. 7. The IC upper bound on the annihilation cross section is expected to scale like  $\sigma_{4e} \rightarrow \sigma_{4e}/(\bar{J}/\bar{J}_0)$ , so that smaller values of  $\bar{J}/\bar{J}_0$  correspond to a weaker bound. One observes that it is not easy to weaken the bound while remaining within the expectations of  $N$ -body simulations. To achieve a factor of 2 reduction would require  $\alpha \simeq 0.22$  and  $r_s = 30$ , for example, which appear to be extreme values.

One can get analytic insight into the dependence of  $\bar{J}$  on  $\alpha$  and  $r_s$  by hypothesizing that  $\bar{J}$  scales like

$$\frac{\bar{J}}{\bar{J}_0} \cong \left( \frac{\rho_0(r_{\text{IC}})}{\rho(r_{\text{IC}})} \right)^2 \quad (15)$$

where  $\rho_0$  is the Einasto profile using the fiducial  $\alpha = 0.17$  and  $r_s = 20$  kpc values, and  $r_{\text{IC}}$  is some characteristic radius that should be of order  $r_\odot$  times the angular displacement (*i.e.*,  $5^\circ$ ) from the galactic center of the relevant solid angular region. By tuning  $r_{\text{IC}}$  to the value 1.75 kpc, we are able to get good agreement with the numerical results, with less than 4% error in the region  $\alpha > 0.15$  (and less than 6% elsewhere). The approximation is shown as the dashed curves in figure 7.

### 3. Potential for strengthening of IC constraint

As we noted above, the current constraints are based on a region that excludes the central latitudes  $|b| < 5^\circ$ , due to the complexity of the disk of the galaxy. On the other hand we know that the strongest bounds arise from the innermost regions. It is therefore interesting to try to project how much stronger the constraints might become if one had made use of the Fermi/LAT  $\gamma$  ray data from the inner latitudes. It is straightforward to recompute the  $J$  factors over regions that include the inner  $\pm 5^\circ$  of latitude to try to project how much stronger the bounds might become. We show the result in fig. 8. According to this extrapolation, the bound could get stronger by a factor of 2 at the reference values of  $\alpha = 0.17$  and  $r_s = 20$  kpc. However this is merely suggestive, and one would have to analyze the actual Fermi  $\gamma$ -ray data in the inner region to draw firm conclusions.

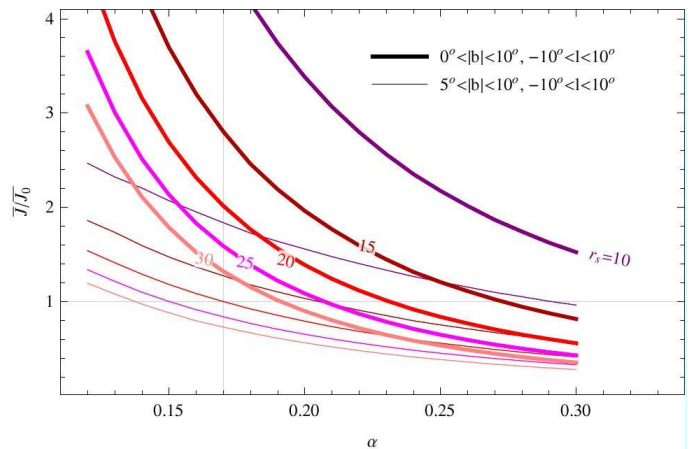


FIG. 8: Solid curves:  $J$  factors as in fig. 7, but averaged over the angular region including the inner latitudes of the galaxy. Dashed curves are for the original region considered in figure 7, for comparison.

## V. OTHER CONSTRAINTS

As mentioned above, a number of complementary constraints have been studied pertaining to models of annihilating DM. We present here the most significant of them, and discuss how they apply to the cases in which we are interested and their impact on the parameter space.

### A. GC gamma ray constraints

Fluxes of gamma rays are directly produced by the DM annihilation process itself ('prompt' gamma rays), mainly from the bremsstrahlung of charged particles and the fragmentation of hadrons, *e.g.*,  $\pi^0$ , produced in the annihilations. These fluxes extend to very high energy (up to the mass of the annihilating DM particle) and are therefore better constrained by comparing the predicted flux with the observations of high energy gamma ray telescopes such as the H.E.S.S. or VERITAS (Very Energetic Radiation Imaging Telescope Array System) observatories. Refs. [9] and [8, 17] have indeed carried out the analysis of these constraints on the parameter space of models that aim to explain the lepton anomalies. H.E.S.S. observations of the region of the Galactic Center [71] (defined as a disk of radius  $0.1^\circ$  centered at the GC), of the Galactic Ridge [72] (defined as a region of  $0.8^\circ \times 0.3^\circ$  in longitude and latitude centered at the GC) and of satellite dwarf spheroidal galaxies such as Sagittarius, Draco, Ursa Minor or Willman 1 [73] impose constraints that can be significant (see [8, 9, 17]).

However, all of these constraints are very sensitive to the details of the chosen DM profile. In particular, for the Milky Way ones, it is the inner part of the galactic DM halo which counts, and numerical simulations do not provide direct determinations of the profile at  $r \sim 100$

pc. Moreover, assuming that an extrapolation is possible, only for the steepest of the profiles that we consider (small  $\alpha$  values) do these bounds become competitive with those from IC, and such values are anyway disfavored by the more robust IC constraints. We therefore need not consider these bounds any further.

### B. GC radio constraint

The  $e^\pm$  produced by DM annihilations within the galactic magnetic field emit synchrotron radiation, which falls in a range of frequencies roughly spanning the radio to the IR. The Galactic Center is the best region to search for this effect, both because of the large local value of the DM density and of the magnetic fields. We do not enter here into the details of the needed astrophysical and particle physics ingredients but refer to [9] for the complete discussion. There, in brief, the signal is computed neglecting advection and diffusion but scanning different (extremal) assumptions for the galactic magnetic field. Ref. [8] has in particular considered the case of the 4-lepton annihilation final state that we are interested in.

Comparing the predicted flux with observations produces constraints on the DM annihilation cross section. Since the observed GC microwave spectrum is harder than what DM annihilations can produce, the dominant bound is obtained considering the observation available at the lowest observed frequency,  $\nu = 0.408$  GHz, performed by [74] in a region with full width half maximum of  $4''$ , corresponding to about 0.1 pc. The resulting bounds can be quite stringent (see [8]) and the constraint extends to low DM masses where the  $\gamma$ -ray bounds from H.E.S.S., discussed above, are not effective. The variation of the magnetic field negligibly affects the bound, because the radio emission is predominantly produced by outer regions. A subdominant bound comes from the VLT observation [75] at the larger infrared/visible frequency from a region with even smaller angular size  $0.04''$  *i.e.*,  $r < 0.0016$  pc. This bound somewhat depends on the magnetic field profile, and it becomes numerically significant only for spiked DM density profiles [76].

However the same discussion as above applies to these bounds: as for the GC gamma ray constraints, these bounds are very sensitive to the details of the chosen DM profile (they originate from the even smaller regions of  $r \sim 1$  pc around the GC) and do not apply to non-steep profiles. We therefore need not consider these bounds any further.

### C. Reionization constraint from CMB

The flux of energy injected by DM annihilation, from the recombination epoch until today through the formation history of DM halos, results in ionization and heating of the intergalactic medium. The ionization and heating can be produced both by the highly energetic ‘prompt’

photons directly emitted in the annihilation of two DM particles, and by the lower energy photons produced by inverse Compton scattering. The latter turns out to be by far the most important process; in fact, the cross section for  $\gamma e^-$  scattering decreases rapidly with the energy of the impinging photon, so that low energy photons are more efficient in removing the electrons from the atoms. These ‘primary reionization’ electrons then deposit their energy in the intergalactic medium via several other interactions, freeing many more electrons and also augmenting the temperature of the gas. One way to constrain DM annihilation properties is therefore to look at the modifications of the CMB spectrum produced by the fact that the CMB photons meet an opaque medium (with free electrons produced by the ionization) in their journey from the surface of last scattering. This is in particular encoded in the total optical depth of the Universe  $\tau$  parameter.  $\tau$  is measured by WMAP to be  $\tau = 0.084 \pm 0.016$  [77], of which about 0.038 is due to the low-redshift reionization ( $z < 6$ ) produced by stars. A DM-induced optical depth larger than 0.062 (the  $1\sigma$  upper bound of [77]) is therefore excluded by these arguments.

This bound has been studied in the literature in several references [21–25], with mutually consistent results. The fit to the numerical result in [24] is

$$\log \sigma_{\text{CMB}} v = -26.3 + 1.15 \log M \quad (16)$$

where  $\sigma v$  is in  $\text{cm}^3/\text{s}$  and  $M$  is in GeV. While this was originally computed for 2-lepton final states, it applies equally well for the 4-lepton ones in which we are interested. All that matters is the total amount of energy that is injected in the primordial intergalactic gas in the form of “electromagnetically coupled” final products (electrons, positrons, photons, possibly hadrons, but not neutrinos). All such final products end up causing reionization and thus producing free electrons, regardless of the precise way in which the annihilation occurs. We neglect minor differences possibly introduced by the difference in the shape of the spectra. The dotted lines in fig. 1 and 11 show these bounds. What one sees is that, for the  $4e$  case in which we are interested, they rule out the large DM mass portion of the PAMELA-only fit region, but not the PAMELA+Fermi one.

In the present work, we consider the case where the annihilating DM constitutes a fraction  $1/f$  of the total DM. Since the annihilation rate scales like  $\rho^2 \sigma$ , the bound (16) will be weakened by  $\sigma_{\text{CMB}} \rightarrow f^2 \sigma_{\text{CMB}}$ .

### D. Extragalactic gamma ray constraints

Finally, we briefly review the extragalactic gamma ray constraints on DM annihilation. These refer to the fluxes of prompt and inverse Compton gamma rays that are produced by annihilations in all DM halos outside of our own galaxy and throughout the history of cosmological structure formation. They reach us (properly redshifted)

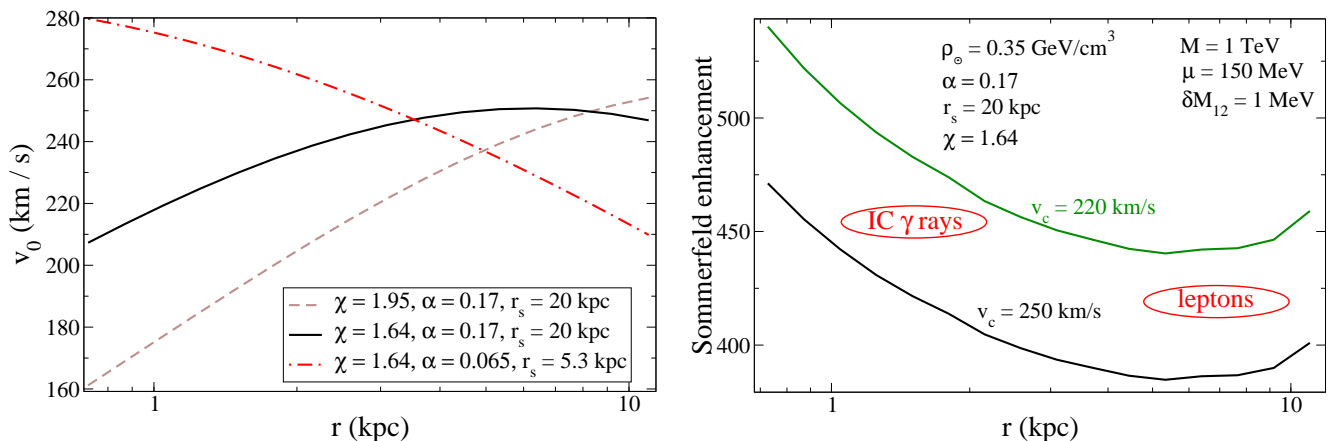


FIG. 9: (a) Left: circular velocity (17) as a function of  $r$  for exponents  $\chi = 1.64$  (includes effects of baryons) and  $\chi = 1.95$  (pure dark matter) at standard Einasto parameters  $\alpha = 0.17$  and  $r_s = 20$  kpc, and for a very cuspy profile (dot-dashed curve). (b) Right: velocity-averaged Sommerfeld enhancement as a function of  $r$  for two different values of the circular velocity  $v_c \equiv v_0(r_\odot)$ . The ellipses denote regions in  $r$  where the dominantly observed IC  $\gamma$  rays and respectively leptons are produced.

uniformly from all directions, so that they have to be compared with the Fermi measurements of isotropic diffuse gamma rays [78]. A number of references have gone through this analysis [19, 20, 26, 27], showing that the bounds depend very significantly on assumptions about the parameters of the history of structure formation. *E.g.*, for conservative choices of the halo concentration parameter function, all of the parameter space in which we are interested is allowed by these bounds.

## VI. RECONCILING ANOMALOUS LEPTONS WITH $\gamma$ -RAY CONSTRAINTS

We have now discussed most of the necessary ingredients for scanning over the parameters of the theoretical models and of the DM density and velocity distributions, to see if there exist any choices that are consistent with all the observational requirements. It remains to explain some details of our methodology for predicting the effective annihilation cross sections, both for the lepton signal and for the IC  $\gamma$  ray signal. These can differ from each other somewhat because of the fact that most of the observed leptons are produced within 1 kpc of the Sun, whereas the most important IC  $\gamma$  rays come from closer to the galactic center, and the Sommerfeld enhancement of the cross section is position dependent. We explain these details in the present section, and use them to obtain the final results.

### A. Position dependence of enhancement factor

As explained above eq. (10), the Sommerfeld enhancement must be averaged over the phase space of the DM. Previously we only considered this in the vicinity of the Sun, but now we must take into account that the average

DM velocity as well as the escape velocity depend upon  $r$ . This dependence has been measured in  $N$ -body simulations, and is shown to follow a scaling relation predicted by Bertschinger [79],

$$v_0(r)^3 \propto r^\chi \rho(r) \quad (17)$$

where the exponent  $\chi \cong 1.9 - 2.0$  for pure DM simulations [32], and it takes lower values  $\chi \cong 1.60 - 1.67$  in simulations including baryons [60]. The  $r$ -dependence of the escape velocity is estimated as in eq. (9). We plot the  $r$ -dependence of  $v_0$  for the standard  $\alpha = 0.17$ ,  $r_s = 20$  kpc profile, normalized so that  $v_0 = 250$  at  $r = r_\odot$  (the latter choice does not effect the shape of  $r$ -dependence) in figure 9(a). The shape is strongly dependent upon the choice of  $\chi$ , with the larger  $\chi$  values giving rise to more pronounced dependence of  $v_0$  upon  $r$ .

Our choice of  $v_0(r)$  differs from one adopted by other authors [63],  $v_0(r) \sim r^{-1/4}$ , that rises as  $r \rightarrow 0$ . The  $r^{-1/4}$  ansatz was inferred from looking at fig. 2 of ref. [64], one of the earlier studies of the effects of baryons on the halo properties. (It should be noticed however that even in this figure, the logarithmic slope of the  $z = 0$  velocity profile does not remain constant as  $r \rightarrow 0$ , but starts to turn downward as in our fig. 9(a).) Based on the more detailed study [60], we infer that the apparent continued rise of  $v_0$  toward  $r = 0$  is consistent with our choice (17) if one also adopts the cuspy profiles found by the simulations that include baryons. To illustrate this, we plot an example in fig. 9(a) (dot-dashed curve) using the steepest profile found in the  $N$ -body simulation with baryons of ref. [60], with  $\alpha = 0.065$  and  $r_s = 5.3$  kpc. The upshot is that eq. (17) predicts that  $v_0(r)$  will always reach a maximum at some  $r = r_{\max}$  and thereafter fall off as  $r \rightarrow 0$ , but the value of  $r_{\max}$  is smaller for cuspy halos. In the present work, we will find that cuspy halos are not consistent with satisfying the inverse Compton constraint, so the  $v_0(r) \sim r^{-1/4}$  would not be

the appropriate one for us to use.

The  $r$ -dependence of  $v_0$  gives rise to  $r$ -dependence in the velocity-averaged enhancement factor  $\langle S \rangle$  eq. (10) [45]. We illustrate for two different values of the circular velocity at the solar radius,  $v_c = v_0(r_\odot) = 220$  and 250 km/s, adopting the exponent  $\chi = 1.64$  which is in the middle of the range for DM simulations including baryons. The enhancement factor is stronger near the galactic center than at the Sun, implying that IC  $\gamma$  rays are produced more copiously relative to leptons than would be the case for a spatially constant boost factor. This is illustrated in figure 9(b) where  $\langle S(r) \rangle$  is plotted. As a result, the IC bound constrains the models more strongly than if one ignored this effect. Like for  $v_0(r)$ , the shape of  $\langle S(r) \rangle$  is nearly independent of the value of  $v_c$ , but depends strongly on the choice of exponent  $\chi$ . Had we chosen the pure DM value  $\chi = 1.9$ , we would get a much stronger ratio of  $\langle S \rangle$  in the galactic center versus solar regions, which would make the IC constraint even more difficult to satisfy.

### B. Estimation of lepton and IC $\gamma$ -ray signals

Our procedure now is to define the cross section for production of  $e^\pm$  (and below, that of IC  $\gamma$  rays), using the partial cross section (5) and enhancement factors that have been averaged over the appropriate regions of space. The average is done with a weighting factor of  $r^2 \rho^2$ , appropriate for annihilations occurring in a shell of radius  $r$  and thickness  $dr$  centered on the sun. Assuming that the observed leptons have diffused no further than  $\Delta r = 1$  kpc [80], the leptonic enhancement factor is

$$B_{e^\pm} = \frac{\int_{r_\odot - \Delta r}^{r_\odot + \Delta r} dr r^2 \rho^2(r) \langle S(r) \rangle}{\int_{r_\odot - \Delta r}^{r_\odot + \Delta r} dr r^2 \rho^2(r)} \quad (18)$$

and the leptonic cross section is  $\sigma_{e^\pm} = b_{11} B_{e^\pm} \sigma_0 f$ , where  $\sigma_0$  is the reference cross section that would give the correct relic density,  $\sigma_0 v = 3 \times 10^{-26} \text{ cm}^3/\text{s}$ . The resulting  $\sigma_{e^\pm} v$  is then compared to the PAMELA and Fermi allowed regions from [17], rescaled by  $(\rho_{\odot,0}/\rho_\odot)^2 f^2$  if necessary. (We do not apply a correction factor for changing  $\alpha$  or  $r_s$  as in the case of the IC constraint, because the behavior of  $\rho(r)$  in the vicinity of  $r_\odot$  does not change significantly as a function of  $\alpha$  or  $r_s$ .) This tells us if the predicted leptonic signal is sufficiently close to the observed one.

For the IC  $\gamma$  ray signal we follow a similar approach, but now  $\langle S(r) \rangle$  should be averaged over a radial interval that corresponds to the path followed by the relevant  $\gamma$  rays. Since the IC signal arrives along a line of sight rather than from a fixed volume, the weighting factor is  $\rho^2$  rather than  $r^2 \rho^2$ . We thus take

$$B_\gamma = \frac{\int_{r_i}^{r_\odot} dr \rho^2(r) \langle S(r) \rangle}{\int_{r_i}^{r_\odot} dr \rho^2(r)} \quad (19)$$

where  $r_i = \tan(5^\circ) r_\odot = 0.73 \text{ kpc}$  is a cutoff due to the fact that the skymap in fig. 3 does not use the inner  $5^\circ$  for setting the IC bounds. The predicted  $\gamma$  ray signal corresponds to the cross section  $\sigma_\gamma = b_{11} B_\gamma \sigma_0 f$ . This should be below the bound

$$\sigma_\gamma < \sigma_{4e} \left( \frac{\rho_{\odot,0}}{\rho_\odot} \right)^2 \left( \frac{\bar{J}_0}{J} \right) f^2 \quad (20)$$

implied by eqs. (12,13,15).

### C. Search of parameter space

We have surveyed the predictions of the models for a range of DM halo parameters  $\rho_\odot$ ,  $\alpha$ ,  $r_s$ ,  $v_c$  in search of examples that can satisfy all the constraints. There are two principal challenges to confront. First, as we illustrated in fig. 2, the Sommerfeld enhancement tends to be too large to fit the lepton signals, especially if the mass splitting is nonzero. Second, the IC constraint rules out large boost factors unless the DM halo parameters are taken to be noncuspy, *i.e.*, large values of  $\alpha$  and  $r_s$ . On the other hand,  $N$ -body simulations favor smaller values of  $\alpha \cong 0.16 - 0.17$  for galaxies of the size of the Milky Way [32, 65, 81].

The upshot is that a compromise must be made: to avoid extremely large values of  $\alpha$ , one needs to marginally satisfy the IC constraint by making the annihilation rate as small as possible, which also pushes the lepton signal to the lower boundary of its allowed region. In order to achieve this reduction in the annihilation rate, we are forced to assume that the annihilating DM only constitutes the fraction  $1/f$  of the total mass density, by increasing the gauge coupling as in (4) to suppress the relic density. Since the Sommerfeld enhancement rises as a function of the mass splitting, there is a trade-off between the parameters  $f$  and  $\delta M$ .

We illustrate the best-case scenarios in figure 10 for the triplet DM model with  $\delta M = 0$  and  $\delta M = 1 \text{ MeV}$ , which shows the model predictions for  $\sigma_{e^\pm} v$  and the  $3\sigma$  confidence level allowed values for PAMELA/Fermi for the two cases. In the first case a sufficiently small annihilation rate is found using the maximum DM fraction  $1/f = 0.4$ , while in the second, it must be reduced to the level of  $1/7$ . These examples illustrate the optimal compromise for satisfying the IC constraint; we are able to just accommodate it using the large, noncuspy Einasto parameter choices  $\alpha = 0.20$ ,  $r_s = 30 \text{ kpc}$ .<sup>6</sup> The lepton rate is barely consistent with the PAMELA/Fermi allowed region for a DM mass of 800 TeV. The relatively low circular velocity  $v_c = 220 \text{ km/s}$  we have adopted also helps to satisfy the IC bound, since as figure 9 implies,

<sup>6</sup> Ref. [82] also finds  $\alpha = 0.20$  in a recent fit to the data including  $\gamma$  rays.



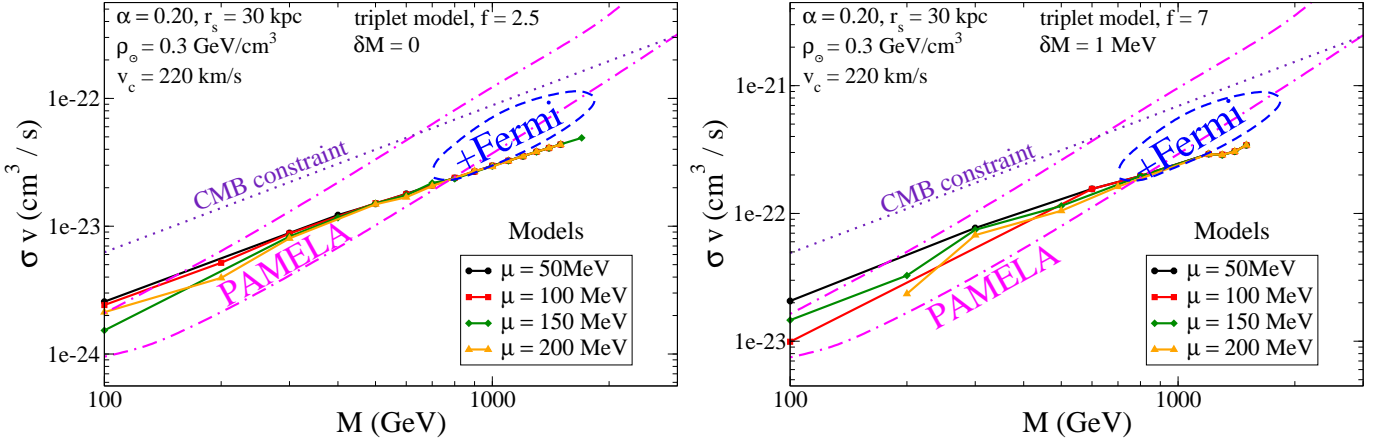


FIG. 10: Predicted and allowed values of  $\sigma v$  versus  $M$  for triplet DM with gauge boson mass  $\mu = 50, 100, 150$  or  $200$  MeV, and halo parameters  $\alpha = 0.20$ ,  $r_s = 30$  kpc,  $\rho_0 = 0.3$  GeV/cm<sup>3</sup>. Only predicted values consistent with IC constraint are shown. Left: mass splitting  $\delta M = 0$ , DM fraction  $1/f = 0.4$ ; right  $\delta M = 1$  MeV,  $1/f = 1/7$ .

the ratio  $B_\gamma/B_{e^+}$  is somewhat smaller for low  $v_c$  than for high  $v_c$ .

To highlight the sensitivity of the IC constraint and lepton signal to the cusiness of the halo profile, we present results of our search using the neighboring Einasto parameters  $\alpha = 0.17, 0.25$  and the triplet DM model, in figure 11. The left-hand panels are similar to fig. 10, while the right hand ones plot the ratio of  $\sigma_\gamma$  to the IC bound (20). The points above the dashed line in the right-hand panels are ruled out by the IC bound, and the figures show how this becomes more severe for smaller  $\alpha$ . The left panels also show the CMB constraint from reionization of the early universe; this is satisfied by a much wider margin than is the IC constraint, as already anticipated. Figure 11 illustrates that for the usually preferred choice  $\alpha = 0.17$ , only compatibility with PAMELA can be achieved, but not simultaneously with the Fermi lepton anomaly. Only models with  $M \lesssim 700$  GeV are consistent with the IC constraint, whose strength is an increasing function of  $M$ .

The tension we find here is not ameliorated by considering the doublet DM model instead of the triplet. Given that the gauge couplings  $\alpha_g$  and cross-section ratios  $b_{11}$  are rather different between the two models, their predictions are surprisingly similar. (This is partly understandable in that we adjust the tree-level cross sections of the two models to be the same, but the Sommerfeld enhancement introduces extra dependence upon  $\alpha_g$ , so there seems to be an accidental cancellation of the effect of  $b_{11}$  by the increase in the Sommerfeld boost.) Moreover the dependence upon the halo parameters is very similar between the two models. In fig. 12 we show the predictions and constraints on  $\sigma v$  versus  $M$  for the doublet model, using the  $\delta M = 1$  MeV mass splitting, and two of the same sets of halo parameters (the less cuspy ones) as we considered for the triplet model. The results are difficult to distinguish from those of the triplet model.

## VII. DISCUSSION

We have tried to carefully assess the likelihood that some of the best theoretically motivated models of annihilating multistate dark matter can explain the PAMELA/Fermi/H.E.S.S. lepton excesses, considering important details of the models whose implications could be missed by a more generic, model-independent investigation. As well, we take into account simulations and observations of the DM halo properties, which have a crucial impact on the viability of the scenario. The main challenge to the models is the difficulty of satisfying constraints from Fermi due to the production of inverse Compton (IC)  $\gamma$  rays produced by the high-energy leptons scattering on galactic radiation.

Among the most important model-dependent features, which affect the ease of satisfying the constraints, are that each annihilation produces two dark gauge bosons, hence four leptons, and these are all  $e^\pm$  as opposed to heavier charged particles if the gauge boson masses are lighter than  $\sim 210$  MeV. The IC constraints for this case are less severe than for models that produce only two leptons, or ones that produce  $\mu^\pm$  in addition to  $e^\pm$ . Moreover the gauge coupling is bounded from below by the requirement that the relic density not exceed what is observed. We find that the boost factor from Sommerfeld enhancement is too large to satisfy the constraints, unless the density of the annihilating DM is suppressed by a factor  $1/f < 0.4$ ; hence one would need an additional component of nonleptophilic DM to make up the rest. Using recent results for the Sommerfeld enhancement factor of multistate DM [38], this problem is exacerbated when the mass splitting is nonzero; one needs  $1/f \sim 0.14 - 0.2$  if  $\delta M \sim 1$  MeV.

A main result is that the Einasto parameters which determine the shape of the DM halo must take large values  $\alpha \gtrsim 0.20$  and  $r_s \sim 30$  kpc in order to barely satisfy the

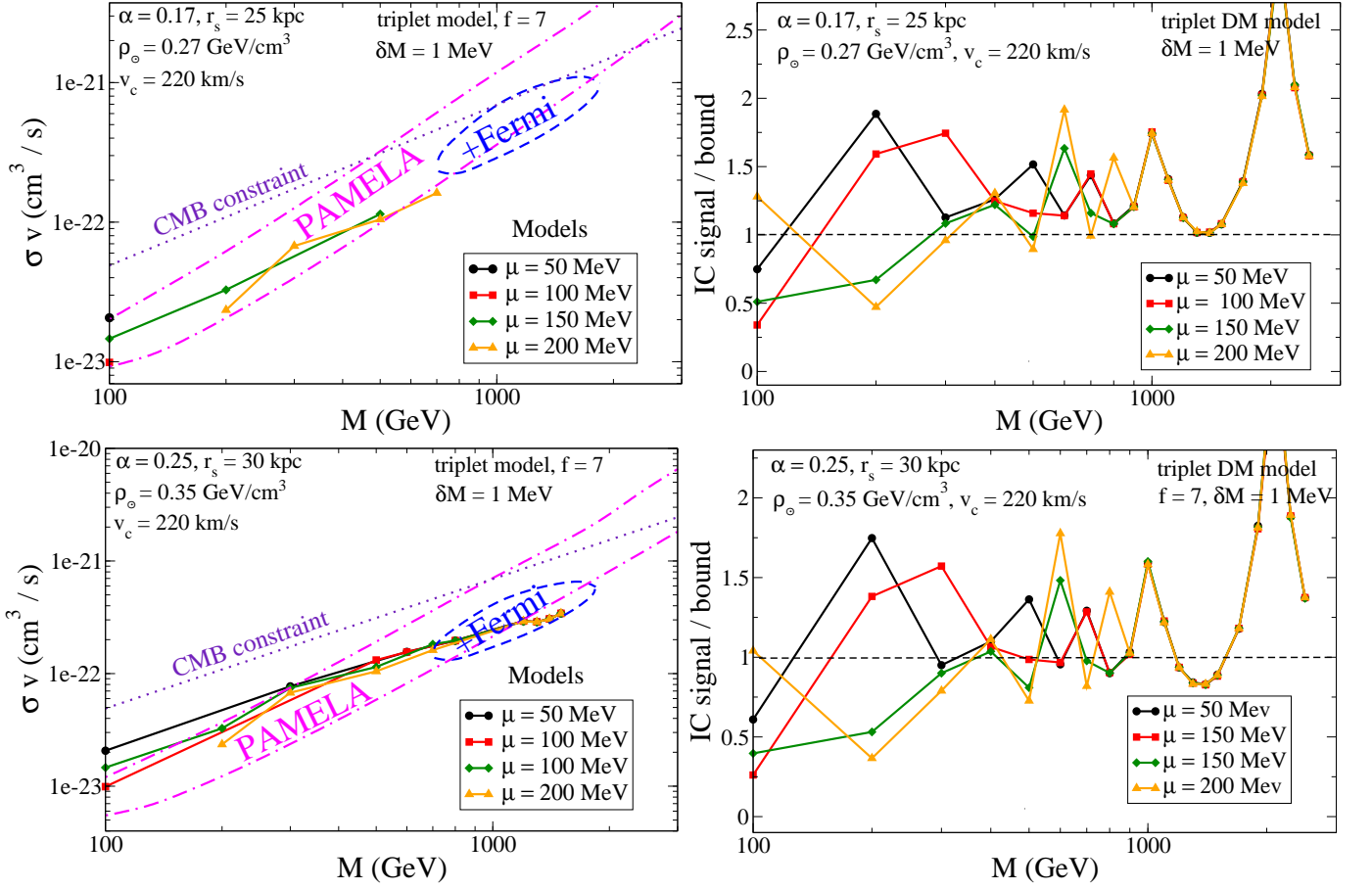


FIG. 11: Left: Predicted and allowed values of  $\sigma v$  versus  $M$  for triplet DM with gauge boson mass  $\mu = 50, 100, 150$  or  $200$  MeV,  $\delta M = 1$  MeV, and DM density fraction  $1/f = 1/7$ . Only the model predictions that are consistent with the IC constraint are shown. Right: ratio of predicted versus maximum allowed IC  $\gamma$  ray cross section for same models. Top row:  $\alpha = 0.17$ ,  $r_s = 25$  kpc, and  $\rho_\odot = 0.27$   $\text{GeV}/\text{cm}^3$ ; bottom row:  $\alpha = 0.25$ ,  $r_s = 30$  kpc and  $\rho_\odot = 0.35$   $\text{GeV}/\text{cm}^3$ .

IC constraint and have marginal consistency with the observed lepton excesses. In the context of pure dark matter simulations, such a large value of  $\alpha$  is above the norm for a galaxy of the size of the Milky Way. Ref. [81] finds a correlation between  $\alpha$  and the virial mass of galaxies  $M_{\text{vir}}$ ,  $\alpha = 0.155 + 0.0095 \nu^2$ , where  $\nu = \delta_{\text{crit}}(z)/\sigma(M_{\text{vir}})$  are functions arising in the Press-Schechter formalism [83] such that  $\delta_{\text{crit}} = 1.686$  at redshift  $z = 0$ , and  $\sigma > 2$  [84] for a galaxy such as ours with  $M_{\text{vir}} = 10^{12} M_\odot$  [70]. Thus  $\nu < 0.843$ , which implies  $\alpha < 0.162$ . However this is only true for the mean value, and a fluctuation as large as  $\alpha = 0.20$  for a galaxy like ours is possible [85]. On the other hand, recent results incorporating baryons indicate that  $\alpha$  is decreased relative to its pure DM value due to adiabatic contraction, which exacerbates the conflict.

We conclude that there is a distinct tension for annihilating models to consistently account for all the lepton excesses, while it is easier to explain that of PAMELA alone using smaller DM masses  $M < 400$  GeV. A possible loophole that we have not considered here is the suggestion that leptons originating from subhalos of our main

halo could provide a substantial fraction of the observed leptonic excess [54]. If this is the case, the production of IC  $\gamma$  rays from the galactic center would be reduced, providing another way to weaken the constraint. How significant this effect could be is under investigation.

**Acknowledgments.** We thank Fang Chen, Ilias Cholis, Julio Navarro, Pasquale Serpico, Tracy Slatyer and Patricia Tissera for helpful discussions and correspondence. We are especially grateful to Alessandro Strumia for detailed information pertaining to ref. [17]. M.C. thanks the EU Marie Curie Research & Training network “UniverseNet” (MRTN-CT-2006-035863) for support. J.C. is supported by the Natural Sciences and Engineering Research Council (Canada).

#### Appendix A: Cross section ratios for $\chi_1 \chi_1 \rightarrow e^\pm$

In this appendix we compute the ratio of the cross section for ground state DM annihilation into  $4e$  final



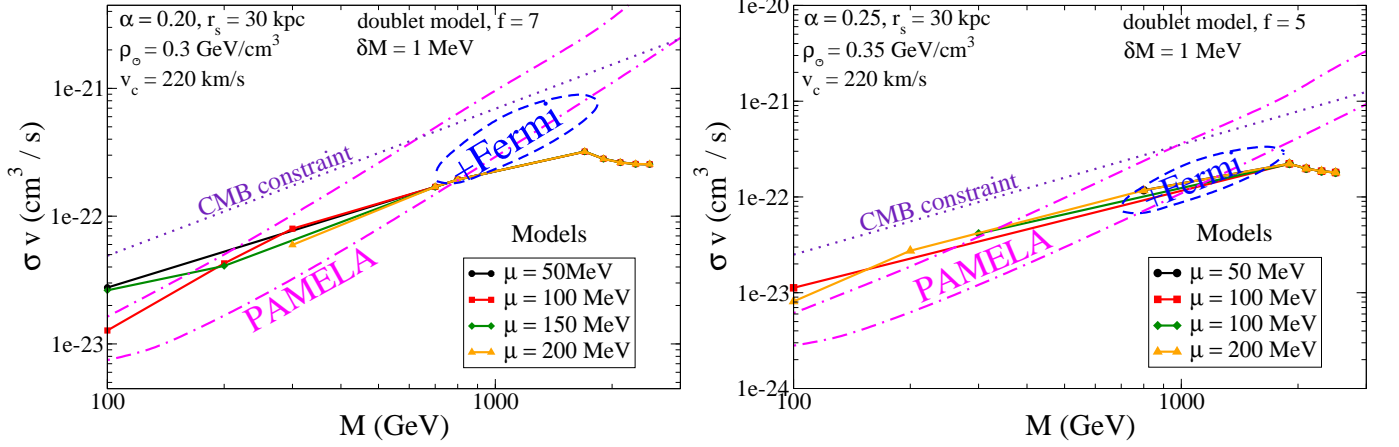


FIG. 12: Same as left panels of fig. 11, but for the doublet DM model. Left:  $\alpha = 0.20$ ,  $r_s = 30$  kpc,  $\rho_\odot = 0.3$  GeV/cm<sup>3</sup>,  $f = 7$ ; Right:  $\alpha = 0.25$ ,  $r_s = 30$  kpc,  $\rho_\odot = 0.35$  GeV/cm<sup>3</sup>,  $f = 5$ .

states relative to the total annihilation cross section in the early universe.

### 1. Triplet model

The total cross section for  $\chi\chi \rightarrow BB$  annihilation was derived for DM in any representation of SU(2) in appendix C of ref. [36]. For the triplet model, the averaged squared matrix element can be expressed in the form  $\frac{1}{3}|\mathcal{M}_{11}|^2 + \frac{2}{3}|\mathcal{M}_{12}|^2$ , where  $|\mathcal{M}_{ij}|^2$  is the matrix element for  $\chi_i\chi_j$ , summed over all possible final states. The factor of  $\frac{1}{3}$  comes from averaging over the colors of  $\chi_j$ . On the other hand, the matrix element for  $\chi_1\chi_1 \rightarrow B_2B_2$  was shown to be just half of  $|\mathcal{M}_{11}|^2$ , since the latter includes  $\chi_1\chi_1 \rightarrow B_3B_3$ . Therefore the ratio  $b_{11}$  for the single process  $\chi_1\chi_1 \rightarrow B_2B_2$  is given by

$$b_{11} = \frac{\frac{1}{2}|\mathcal{M}_{11}|^2}{\frac{1}{3}|\mathcal{M}_{11}|^2 + \frac{2}{3}|\mathcal{M}_{12}|^2} = \frac{\frac{1}{2} \cdot 8}{\frac{1}{3}(8 + 5/2)} = \frac{8}{7} \quad (\text{A1})$$

using the results of [36] for the matrix elements. In units of  $g^4$ ,  $|\mathcal{M}_{11}|^2 = 2(|t|^2 + |u|^2)$  where  $|t|^2$  and  $|u|^2$  stand for the contributions from the  $t$  and  $u$  channels, respectively, and take the values  $|t|^2 = |u|^2 = 2$ . Likewise  $|\mathcal{M}_{12}|^2 = |t|^2 + |s|^2 + |st|$  with  $|s|^2 = -19/4$  and  $|st| = 4$ . The interference between  $t$  and  $u$  channels vanishes,  $|tu| = 0$ .

### 2. Doublet model

For the doublet model, the matrix element for  $\chi_i\chi_j \rightarrow B_aB_b$  can be expressed in the form

$$\mathcal{M}_{ij}^{ab} = \frac{1}{4}\tau_{jk}^b\tau_{ki}^a t + \frac{1}{4}\tau_{jk}^a\tau_{ki}^b u + \frac{i}{2}\tau_{ji}^c\epsilon^{abc} s \quad (\text{A2})$$

where  $s, t, u$  are the spinor parts of the amplitude in the respective channel. The factors of  $1/2$  are for the normalization of the SU(2) generators. To find the averaged

cross section for the early universe, we sum over  $a, b$  and average over  $i, j$ . This gives

$$\begin{aligned} \langle |\mathcal{M}|^2 \rangle &= \frac{1}{4} \left[ \frac{18}{16} (|t|^2 + |u|^2) + \frac{12}{4} |s|^2 + \frac{12}{8} (|st| + |su|) \right] \\ &= \frac{9}{16} \end{aligned} \quad (\text{A3})$$

where we used the values given above for  $|t|^2$ ,  $|u|^2$ ,  $|s|^2$ ,  $|st|$  and also  $|su| = |st|$ . This expression agrees with the general result  $\langle |\mathcal{M}|^2 \rangle = \frac{3j(j+1)}{2j+1} [j(j+1) - 1/4]$  for the spin- $j$  representation of SU(2) found in [36], when  $j = 1/2$ . We need to compare this result with that of the exclusive channel  $\chi_1\chi_1 \rightarrow B_2B_2$ ,

$$|\mathcal{M}_{11}^{22}|^2 = \frac{1}{16} (|t|^2 + |u|^2) = \frac{1}{4} \quad (\text{A4})$$

The ratio of these would give  $(\frac{1}{4})/(\frac{9}{16}) = 4/9$ . However unlike the triplet model, there is an additional process that can give the  $B_2$  gauge boson, namely  $\chi_1\chi_1 \rightarrow B_1B_2$ , which has

$$\begin{aligned} |\mathcal{M}_{11}^{12}|^2 &= \frac{1}{16} (|t|^2 + |u|^2) + \frac{1}{4} |s|^2 + \frac{1}{8} (|st| + |su|) \\ &= \frac{1}{16} \end{aligned} \quad (\text{A5})$$

This should be doubled to take into account the  $\chi_1\chi_1 \rightarrow B_2B_1$  contribution, but we halve it again to account for the fact that only one  $B_2$  gauge boson is produced, so it gives half as many leptons as the  $B_2B_2$  final state. Hence we find that

$$b_{11} = \frac{\frac{1}{4} + \frac{1}{16}}{\frac{9}{16}} = \frac{5}{9} \quad (\text{A6})$$

## Appendix B: Multistate Sommerfeld enhancement

The Sommerfeld enhancement factor for multicomponent DM annihilation is different from the that of the

single component case. In particular if the gauge couplings are off-diagonal,  $\bar{\chi}_1 \not{B} \chi_2$  and if there is a mass dif-

ference  $\delta M$  between  $\chi_1$  and  $\chi_2$ , ref. [38] finds that the enhancement factor is given by

---


$$S = \frac{2\pi}{\epsilon_v} \sinh\left(\frac{\epsilon_v \pi}{\nu}\right) \begin{cases} \frac{1}{\cosh(\epsilon_v \pi / \nu) - \cos\left(\sqrt{\epsilon_\delta^2 - \epsilon_v^2} \pi / \nu + 2\theta_-\right)} & \epsilon_v < \epsilon_\delta, \\ \frac{\cosh\left(\left(\epsilon_v + \sqrt{-\epsilon_\delta^2 + \epsilon_v^2}\right) \pi / 2\nu\right) \operatorname{sech}\left(\left(\epsilon_v - \sqrt{-\epsilon_\delta^2 + \epsilon_v^2}\right) \pi / 2\nu\right)}{\cosh\left(\left(\epsilon_v + \sqrt{-\epsilon_\delta^2 + \epsilon_v^2}\right) \pi / \nu\right) - \cos(2\theta_-)} & \epsilon_v > \epsilon_\delta. \end{cases} \quad (\text{B1})$$


---

with the definitions  $\epsilon_v = v/(c\alpha_g)$  ( $v$  being the center-of-mass velocity of one of the DM particles),  $\epsilon_\phi = \mu/(M\alpha)$ , and  $\nu = \frac{1}{2}\epsilon_\phi(1 + \sqrt{1 + 4/(\epsilon_\phi r_M)})$ .  $r_M$  is a radial coordinate value defined such that  $V(r_M) = \max(\epsilon_\delta^2/2, \epsilon_\phi^2)$ , where  $\epsilon_\delta = \sqrt{2\delta M/M}/\alpha_g$  and  $V(r) = e^{-\epsilon_\phi r}/r$ .  $\theta_-$  is a function defined as an integral that must be done numerically (see eq. (4.8) and footnote 3 of [38]).

### Appendix C: Escape velocity

In general, the escape velocity from a given radius is given in terms of the gravitational potential

$$\frac{1}{2}v_{\text{esc}}^2 = -\Phi(r) = G \int_r^\infty \frac{dR}{R^2} M(R) \quad (\text{C1})$$

where  $M(r)$  is the mass enclosed within radius  $r$ . If all of the matter in the galaxy was dark, we could simply integrate  $\rho(r)$  to find  $M(r)$ , but baryons constitute a significant fraction of the matter in the inner part of the galaxy, so this would give an underestimate of  $v_{\text{esc}}$ . Instead, one can try to infer the shape of  $M(r)$  from rotation curves, which measure the circular velocity  $v_c(r)^2 = GM(r)/r$ . We thus have the relation

$$v_{\text{esc}}^2 = 2 \int_r^\infty \frac{dr}{r} v_c^2(r) \quad (\text{C2})$$

For flat rotation curves,  $M(r)$  increases linearly with  $r$ , and  $v_{\text{esc}}^2$  goes like  $-\ln(r)$ . Recent observations of the

Milky Way [70] indicate that its circular velocity is nearly constant to a radius of  $r_{10} \equiv 10$  kpc, and falls slowly like  $r^{p-1}$  between  $r_{10}$  and 60 kpc, where  $p < 1$ . This corresponds to  $M(r) \sim r^{2p-1}$  in the region between 10 and 60 kpc. Since  $v_c$  falls from 200 km/s at  $r_{10}$  to 170 km/s at 60 kpc, we infer that  $p = 0.856$ . This tells us that  $v_c = 220$  km/s for  $r < r_{10}$  and  $v_c = (220 \text{ km/s}) \times (r/r_{10})^{p-1}$  in the region between  $r_{10}$  and 60 kpc.

We still need an estimate of how  $v_c$  behaves at  $r > 60$  kpc in order to do the integral (C2). The most radical assumption would be that there is no more mass beyond this radius, so that  $v_c$  drops like  $1/\sqrt{r}$  beyond this point. However, the appearance of the rotation curve at the highest measured radii does not suggest such a change; moreover we have an estimate of the total mass of the galaxy through its virial mass  $M_{\text{vir}}$ , determined to be  $10^{12} M_\odot$  in ref. [70]. Therefore it would seem reasonable to assume that  $M(r)$  continues to grow with the same power law  $r^{2p-1}$  out to a radius that contains  $M_{\text{vir}}$ , after which it stops growing. In the present case that radius corresponds to  $r_{\text{vir}} = 175$  kpc. We therefore take  $r_{\text{vir}}$  as our estimate of where  $M(r)$  ceases to grow. In the region  $r < r_{10}$ , this gives

$$v_{\text{esc}}^2 = 2v_c^2 \left[ \ln\left(\frac{r_{10}}{r}\right) + \frac{1}{2(1-p)} \left( 1 + (1-2p) \left(\frac{r_{10}}{r_{\text{vir}}}\right)^{2(1-p)} \right) \right] \quad (\text{C3})$$

- 
- [1] O. Adriani *et al.* [PAMELA Collaboration], “An anomalous positron abundance in cosmic rays with energies 1.5–100 GeV,” *Nature* **458**, 607 (2009) [arXiv:0810.4995 [astro-ph]].
  - [2] A. A. Abdo *et al.* [The Fermi LAT Collaboration], “Measurement of the Cosmic Ray  $e^+$  plus  $e^-$  spectrum from 20 GeV to 1 TeV with the Fermi Large Area Telescope,” *Phys. Rev. Lett.* **102**, 181101 (2009) [arXiv:0905.0025 [astro-ph.HE]].
  - [3] F. Aharonian *et al.* [H.E.S.S. Collaboration], “The energy spectrum of cosmic-ray electrons at TeV energies,” *Phys. Rev. Lett.* **101**, 261104 (2008) [arXiv:0811.3894 [astro-

ph]];

“Probing the ATIC peak in the cosmic-ray electron spectrum with H.E.S.S.,” *Astron. Astrophys.* **508**, 561 (2009) [arXiv:0905.0105 [astro-ph.HE]].

- [4] M. Cirelli, M. Kadastik, M. Raidal and A. Strumia, “Model-independent implications of the  $e^+$ ,  $e^-$ , anti-proton cosmic ray spectra on properties of Dark Matter,” *Nucl. Phys. B* **813** (2009) 1 [arXiv:0809.2409 [hep-ph]].
- [5] F. Donato, D. Maurin, P. Brun, T. Delahaye and P. Salati, “Constraints on WIMP Dark Matter from the High Energy PAMELA  $\bar{p}/p$  data,” *Phys. Rev. Lett.* **102**, 071301 (2009) [arXiv:0810.5292 [astro-ph]].

- [6] I. Cholis, G. Dobler, D. P. Finkbeiner, L. Goodenough and N. Weiner, “The Case for a 700+ GeV WIMP: Cosmic Ray Spectra from ATIC and PAMELA,” *Phys. Rev. D* **80** (2009) 123518 [arXiv:0811.3641 [astro-ph]].
- [7] L. Bergstrom, J. Edsjo and G. Zaharijas, “Dark matter interpretation of recent electron and positron data,” *Phys. Rev. Lett.* **103**, 031103 (2009) [arXiv:0905.0333 [astro-ph.HE]].
- [8] P. Meade, M. Papucci, A. Strumia and T. Volansky, “Dark Matter Interpretations of the Electron/Positron Excesses after FERMI,” arXiv:0905.0480 [hep-ph].
- [9] G. Bertone, M. Cirelli, A. Strumia and M. Taoso, “Gamma-ray and radio tests of the  $e+e-$  excess from DM annihilations,” *JCAP* **0903**, 009 (2009) [arXiv:0811.3744 [astro-ph]].
- [10] L. Bergstrom, G. Bertone, T. Bringmann, J. Edsjo and M. Taoso, “Gamma-ray and Radio Constraints of High Positron Rate Dark Matter Models Annihilating into New Light Particles,” *Phys. Rev. D* **79**, 081303 (2009) [arXiv:0812.3895 [astro-ph]].
- [11] P. Meade, M. Papucci and T. Volansky, “Dark Matter Sees The Light,” *JHEP* **0912**, 052 (2009) [arXiv:0901.2925 [hep-ph]].
- [12] R. M. Crocker, N. F. Bell, C. Balazs and D. I. Jones, “Radio and gamma-ray constraints on dark matter annihilation in the Galactic center,” *Phys. Rev. D* **81**, 063516 (2010) [arXiv:1002.0229].
- [13] M. Cirelli and P. Panci, “Inverse Compton constraints on the Dark Matter  $e+e-$  excesses,” *Nucl. Phys. B* **821**, 399 (2009) [arXiv:0904.3830 [astro-ph.CO]].
- [14] E. Borriello, A. Cuoco and G. Miele, “Secondary radiation from the Pamela/ATIC excess and relevance for Fermi,” *Astrophys. J.* **699**, L59 (2009) [arXiv:0903.1852 [astro-ph.GA]].
- [15] M. Regis and P. Ullio, “Testing the Dark Matter Interpretation of the PAMELA Excess through Measurements of the Galactic Diffuse Emission,” arXiv:0904.4645 [astro-ph.GA].
- [16] I. Cholis, G. Dobler, D. P. Finkbeiner, L. Goodenough, T. R. Slatyer and N. Weiner, “The Fermi gamma-ray spectrum of the inner galaxy: Implications for annihilating dark matter,” arXiv:0907.3953 [astro-ph.HE].
- [17] M. Papucci and A. Strumia, “Robust implications on Dark Matter from the first FERMI sky gamma map,” arXiv:0912.0742 [hep-ph].
- [18] M. Cirelli, P. Panci and P. D. Serpico, “Diffuse gamma ray constraints on annihilating or decaying Dark Matter after Fermi,” arXiv:0912.0663 [astro-ph.CO].
- [19] A. A. Abdo *et al.* [Fermi-LAT Collaboration], “Constraints on Cosmological Dark Matter Annihilation from the Fermi-LAT Isotropic Diffuse Gamma-Ray Measurement,” *JCAP* **1004**, 014 (2010) [arXiv:1002.4415].
- [20] G. Hutsi, A. Hektor and M. Raidal, “Implications of the Fermi-LAT diffuse gamma-ray measurements on annihilating or decaying Dark Matter,” arXiv:1004.2036.
- [21] S. Galli, F. Iocco, G. Bertone and A. Melchiorri, “CMB constraints on Dark Matter models with large annihilation cross-section,” *Phys. Rev. D* **80**, 023505 (2009) [arXiv:0905.0003 [astro-ph.CO]].
- [22] T. R. Slatyer, N. Padmanabhan and D. P. Finkbeiner, “CMB Constraints on WIMP Annihilation: Energy Absorption During the Recombination Epoch,” *Phys. Rev. D* **80**, 043526 (2009) [arXiv:0906.1197 [astro-ph.CO]].
- [23] G. Huetsi, A. Hektor and M. Raidal, “Constraints on leptonically annihilating Dark Matter from reionization and extragalactic gamma background,” *Astron. Astrophys.* **505**, 999 (2009) [arXiv:0906.4550 [astro-ph.CO]].
- [24] M. Cirelli, F. Iocco and P. Panci, “Constraints on Dark Matter annihilations from reionization and heating of the intergalactic gas,” *JCAP* **0910**, 009 (2009) [arXiv:0907.0719 [astro-ph.CO]].
- [25] T. Kanzaki, M. Kawasaki and K. Nakayama, “Effects of Dark Matter Annihilation on the Cosmic Microwave Background,” arXiv:0907.3985 [astro-ph.CO].
- [26] S. Profumo and T. E. Jeltema, “Extragalactic Inverse Compton Light from Dark Matter Annihilation and the Pamela Positron Excess,” arXiv:0906.0001 [astro-ph.CO].
- [27] A. V. Belikov and D. Hooper, “The Contribution Of Inverse Compton Scattering To The Diffuse Extragalactic Gamma-Ray Background From Annihilating Dark Matter,” arXiv:0906.2251 [astro-ph.CO].
- [28] J. F. Navarro, C. S. Frenk and S. D. M. White, “The Structure of Cold Dark Matter Halos,” *Astrophys. J.* **462** (1996) 563 [arXiv:astro-ph/9508025].
- [29] K. G. Begeman, A. H. Broeils, R. H. Sanders, *MNRAS* **249**, 523 (1991). J. N. Bahcall and R. M. Soneira, “The Universe At Faint Magnetitudes. 2. Models For The Predicted Star Counts,” *Astrophys. J. Suppl.* **44**, 73 (1980).
- [30] A. Burkert, “The Structure of dark matter halos in dwarf galaxies,” *IAU Symp.* **171** (1996) 175 [*Astrophys. J.* **447** (1995) L25] [arXiv:astro-ph/9504041]. See also: P. Salucci and A. Burkert, “Dark Matter Scaling Relations,” arXiv:astro-ph/0004397, G. Gentile, P. Salucci, U. Klein, D. Vergani and P. Kalberla, “The cored distribution of dark matter in spiral galaxies,” *Mon. Not. Roy. Astron. Soc.* **351** (2004) 903 [arXiv:astro-ph/0403154] and P. Salucci, A. Lapi, C. Tonini, G. Gentile, I. Yegorova and U. Klein, “The universal rotation curve of spiral galaxies. II: The dark matter distribution out to the virial radius,” *Mon. Not. Roy. Astron. Soc.* **378** (2007) 41 [arXiv:astro-ph/0703115].
- [31] A. W. Graham, D. Merritt, B. Moore, J. Diemand and B. Terzić, “Empirical models for Dark Matter Halos. I. Nonparametric Construction of Density Profiles and Comparison with Parametric Models,” *Astron. J.* **132** (2006) 2685 [arXiv:astro-ph/0509417].
- [32] J. F. Navarro *et al.*, “The Diversity and Similarity of Cold Dark Matter Halos,” arXiv:0810.1522 [astro-ph].
- [33] N. Arkani-Hamed, D. P. Finkbeiner, T. R. Slatyer and N. Weiner, “A Theory of Dark Matter,” *Phys. Rev. D* **79**, 015014 (2009) [arXiv:0810.0713 [hep-ph]].
- [34] M. Baumgart, C. Cheung, J. T. Ruderman, L. T. Wang and I. Yavin, “Non-Abelian Dark Sectors and Their Collider Signatures,” *JHEP* **0904**, 014 (2009) [arXiv:0901.0283 [hep-ph]].
- [35] F. Chen, J. M. Cline and A. R. Frey, “A new twist on excited dark matter: implications for INTEGRAL, PAMELA/ATIC/PPB-BETS, DAMA,” *Phys. Rev. D* **79**, 063530 (2009) [arXiv:0901.4327 [hep-ph]].
- [36] F. Chen, J. M. Cline and A. R. Frey, “Nonabelian dark matter: models and constraints,” *Phys. Rev. D* **80**, 083516 (2009) [arXiv:0907.4746 [hep-ph]].
- [37] A. Sommerfeld, “Über die Beugung und Bremsung der Elektronen,” *Ann. Phys.* **403**, 257 (1931). J. Hisano, S. Matsumoto and M. M. Nojiri, *Phys. Rev.*

- Lett. 92 (2004) 031303 [arXiv: hep-ph/0307216].  
 J. Hisano, S. Matsumoto, M. M. Nojiri and O. Saito, Phys. Rev. D **71** (2005) 063528 [arXiv: hep-ph/0412403].  
 M. Cirelli, A. Strumia, M. Tamburini, Nucl. Phys. B **787** (2007) 152 [arXiv:0706.4071 [hep-ph]].  
 M. Lattanzi and J. I. Silk, arXiv:0812.0360 [astro-ph].  
 See also previous work in K. Belotsky, D. Fargion, M. Khlopov and R. V. Konoplich, Phys. Atom. Nucl. **71** (2008) 147 [arXiv:hep-ph/0411093] and references therein.
- [38] T. R. Slatyer, “The Sommerfeld enhancement for dark matter with an excited state,” JCAP **1002**, 028 (2010) [arXiv:0910.5713 [hep-ph]].
- [39] D. Tucker-Smith and N. Weiner, “The status of inelastic dark matter,” Phys. Rev. D **72**, 063509 (2005) [arXiv:hep-ph/0402065].
- [40] J. Knödseder *et al.*, “Early SPI/INTEGRAL constraints on the morphology of the 511 keV line emission in the 4th galactic quadrant,” Astron. Astrophys. **411**, L457 (2003) [arXiv:astro-ph/0309442]; P. Jean *et al.*, “Early SPI/INTEGRAL measurements of galactic 511 keV line emission from positron annihilation,” Astron. Astrophys. **407**, L55 (2003) [arXiv:astro-ph/0309484]. J. Knödseder *et al.*, “The all-sky distribution of 511-keV electron positron annihilation emission,” Astron. Astrophys. **441**, 513 (2005) [arXiv:astro-ph/0506026].
- [41] D. P. Finkbeiner and N. Weiner, “Exciting Dark Matter and the INTEGRAL/SPI 511 keV signal,” Phys. Rev. D **76**, 083519 (2007) [arXiv:astro-ph/0702587].
- [42] M. Pospelov and A. Ritz, “The galactic 511-keV line from electroweak scale WIMPs,” Phys. Lett. B **651**, 208 (2007) [arXiv:hep-ph/0703128].
- [43] F. Chen, J. M. Cline, A. Fradette, A. R. Frey and C. Rabideau, “Exciting dark matter in the galactic center,” arXiv:0911.2222 [hep-ph].
- [44] F. Chen, J. M. Cline, A. R. Frey, “Stable excited dark matter and galactic 511 keV gamma rays,” in preparation
- [45] B. Robertson and A. Zentner, “Dark Matter Annihilation Rates with Velocity-Dependent Annihilation Cross Sections,” Phys. Rev. D **79**, 083525 (2009) [arXiv:0902.0362 [astro-ph.CO]].
- [46] M. Kuhlen, J. Diemand and P. Madau, “The Dark Matter Annihilation Signal from Galactic Substructure: Predictions for GLAST,” arXiv:0805.4416 [astro-ph].
- [47] J. Bovy, “Substructure Boosts to Dark Matter Annihilation from Sommerfeld Enhancement,” Phys. Rev. D **79**, 083539 (2009) [arXiv:0903.0413 [astro-ph.HE]].
- [48] M. Kuhlen, “The Dark Matter Annihilation Signal from Dwarf Galaxies and Subhalos,” arXiv:0906.1822 [astro-ph.GA].
- [49] M. D. Kistler and J. M. Siegal-Gaskins, “Gamma-ray signatures of annihilation to charged leptons in dark matter substructure,” arXiv:0909.0519 [astro-ph.HE].
- [50] S. Ando, “Gamma-ray background anisotropy from galactic dark matter substructure,” Phys. Rev. D **80**, 023520 (2009) [arXiv:0903.4685 [astro-ph.CO]].
- [51] M. Kuhlen, P. Madau and J. Silk, “Exploring Dark Matter with Milky Way substructure,” arXiv:0907.0005 [astro-ph.GA].
- [52] M. Kamionkowski, S. M. Koushiappas and M. Kuhlen, “Galactic Substructure and Dark Matter Annihilation in the Milky Way Halo,” Phys. Rev. D **81**, 043532 (2010) [arXiv:1001.3144 [astro-ph.GA]].
- [53] P. Brun, T. Delahaye, J. Diemand, S. Profumo and P. Salati, “The cosmic ray lepton puzzle in the light of cosmological N-body simulations,” Phys. Rev. D **80**, 035023 (2009) [arXiv:0904.0812 [astro-ph.HE]].
- [54] J. M. Cline, A. C. Vincent and W. Xue, “Leptons from Dark Matter Annihilation in Milky Way Subhalos,” Phys. Rev. D **81**, 083512 (2010) [arXiv:1001.5399 [astro-ph.CO]].
- [55] J. D. Bjorken, R. Essig, P. Schuster and N. Toro, “New Fixed-Target Experiments to Search for Dark Gauge Forces,” Phys. Rev. D **80**, 075018 (2009) [arXiv:0906.0580 [hep-ph]].
- [56] M. J. Reid *et al.*, “Trigonometric Parallaxes of Massive Star Forming Regions: VI. Galactic Structure, Fundamental Parameters and Non-Circular Motions,” Astrophys. J. **700**, 137 (2009) [arXiv:0902.3913 [astro-ph.GA]].
- [57] P. J. McMillan and J. J. Binney, “The uncertainty in Galactic parameters,” arXiv:0907.4685 [astro-ph.GA].
- [58] S. Gillessen, F. Eisenhauer, S. Trippe, T. Alexander, R. Genzel, F. Martins and T. Ott, “Monitoring stellar orbits around the Massive Black Hole in the Galactic Center,” Astrophys. J. **692**, 1075 (2009) [arXiv:0810.4674 [astro-ph]].
- [59] M. C. Smith *et al.*, “The RAVE Survey: Constraining the Local Galactic Escape Speed,” Mon. Not. Roy. Astron. Soc. **379**, 755 (2007) [arXiv:astro-ph/0611671].
- [60] P. B. Tissera, S. D. M. White, S. Pedrosa and C. Scannapieco, “Dark matter response to galaxy formation,” arXiv:0911.2316 [astro-ph.CO].
- [61] M. G. Abadi, J. F. Navarro, M. Fardal, A. Babul and M. Steinmetz, “Galaxy-Induced Transformation of Dark Matter Halos,” arXiv:0902.2477 [astro-ph.GA].
- [62] S. E. Pedrosa, P. B. Tissera and C. Scannapieco, “The joint evolution of baryons and dark matter haloes,” arXiv:0910.4380 [astro-ph.CO].
- [63] I. Cholis and N. Weiner, “MiXDM: Cosmic Ray Signals from Multiple States of Dark Matter,” arXiv:0911.4954 [astro-ph.HE].
- [64] E. Romano-Diaz, I. Shlosman, Y. Hoffman and C. Heller, “Erasing Dark Matter Cusps in Cosmological Galactic Halos with Baryons,” arXiv:0808.0195 [astro-ph].
- [65] J. Stadel *et al.*, “Quantifying the heart of darkness with GHALO - a multi-billion particle simulation of our galactic halo,” arXiv:0808.2981 [astro-ph].
- [66] C. Amsler *et al.* (Particle Data Group), Physics Letters B **667**, 1 (2008)
- [67] R. Catena and P. Ullio, “A novel determination of the local dark matter density,” arXiv:0907.0018 [astro-ph.CO].
- [68] P. Salucci, F. Nesti, G. Gentile and C. F. Martins, “The dark matter density at the Sun’s location,” arXiv:1003.3101 [astro-ph.GA].
- [69] T. Sakamoto, M. Chiba and T. C. Beers, “The Mass of the Milky Way: Limits from a Newly Assembled Set of Halo Objects,” Astron. Astrophys. **397**, 899 (2003) [arXiv:astro-ph/0210508].
- [70] X. X. Xue *et al.* [SDSS Collaboration], “The Milky Way’s Circular Velocity Curve to 60 kpc and an Estimate of the Dark Matter Halo Mass from Kinematics of 2400 SDSS Blue Horizontal Branch Stars,” Astrophys. J. **684**, 1143 (2008) [arXiv:0801.1232 [astro-ph]].
- [71] F. Aharonian *et al.* [The HESS Collaboration], “Very high energy gamma rays from the direction of Sagittarius A\*,” Astron. Astrophys. **425**, L13 (2004) [arXiv:astro-ph/0408145].  
 F. Aharonian *et al.* [H.E.S.S. Collaboration], “HESS ob-

- servations of the galactic center region and their possible dark matter interpretation,” *Phys. Rev. Lett.* **97**, 221102 (2006) [Erratum-ibid. **97**, 249901 (2006)] [arXiv:astro-ph/0610509].
- [72] F. Aharonian *et al.* [H.E.S.S. Collaboration], “Discovery of Very-High-Energy Gamma-Rays from the Galactic Centre Ridge,” *Nature* **439**, 695 (2006) [arXiv:astro-ph/0603021].
- [73] F. Aharonian [HESS Collaboration], “Observations of the Sagittarius Dwarf galaxy by the H.E.S.S. experiment and search for a Dark Matter signal,” *Astropart. Phys.* **29**, 55 (2008) [Erratum-ibid. **33**, 274 (2010)] [arXiv:0711.2369 [astro-ph]].
- C. M. Hui, the VERITAS Collaboration, “VERITAS Observations of Extragalactic Non-Blazars,” *AIP Conf. Proc.* **1085**, 407 (2009) [arXiv:0810.1913 [astro-ph]].
- R. Essig, N. Sehgal and L. E. Strigari, “Bounds on Cross-sections and Lifetimes for Dark Matter Annihilation and Decay into Charged Leptons from Gamma-ray Observations of Dwarf Galaxies,” *Phys. Rev. D* **80**, 023506 (2009) [arXiv:0902.4750 [hep-ph]].
- [74] R.D.Davis, D.Walsh, R.S.Booth, *MNRAS* **177**, 319-333 (1976)
- [75] R. Genzel *et al.*, “Near-infrared flares from accreting gas around the supermassive black hole at the Galactic Centre,” *Nature* **425** (2003) 934 [astro-ph/0310821].
- [76] M. Regis and P. Ullio, “Multi-wavelength signals of dark matter annihilations at the Galactic center,” *Phys. Rev. D* **78**, 043505 (2008) [arXiv:0802.0234].
- [77] E. Komatsu *et al.* [WMAP Collaboration], “Five-Year Wilkinson Microwave Anisotropy Probe (WMAP) Observations: Cosmological Interpretation,” *Astrophys. J. Suppl.* **180** (2009) 330 [arXiv:0803.0547 [astro-ph]].
- [78] A. A. Abdo *et al.* [The Fermi-LAT collaboration], “The Spectrum of the Isotropic Diffuse Gamma-Ray Emission Derived From First-Year Fermi Large Area Telescope Data,” *Phys. Rev. Lett.* **104**, 101101 (2010) [arXiv:1002.3603].
- [79] E. Bertschinger, “Self - similar secondary infall and accretion in an Einstein-de Sitter universe,” *Astrophys. J. Suppl.* **58**, 39 (1985).
- [80] J. Lavalle, E. Nezri, E. Athanassoula, F. S. Ling and R. Teyssier, “Antimatter cosmic rays from dark matter annihilation: First results from an N-body experiment,” *Phys. Rev. D* **78**, 103526 (2008) [arXiv:0808.0332 [astro-ph]].
- J. Lavalle, J. Pochon, P. Salati and R. Taillet, “Clumpiness of Dark Matter and Positron Annihilation Signal: Computing the odds of the Galactic Lottery,” *Astron. Astrophys.* **462**, 827 (2007) [arXiv:astro-ph/0603796].
- [81] L. Gao *et al.*, “The redshift dependence of the structure of massive LCDM halos,” arXiv:0711.0746 [astro-ph].
- [82] T. Lin, D. P. Finkbeiner and G. Dobler, “The Electron Injection Spectrum Determined by Anomalous Cosmic Ray, Gamma Ray, and Microwave Signals,” arXiv:1004.0989 [astro-ph.CO].
- [83] W. H. Press and P. Schechter, “Formation of galaxies and clusters of galaxies by selfsimilar gravitational condensation,” *Astrophys. J.* **187**, 425 (1974).
- [84] A. Loeb, “First Light,” arXiv:astro-ph/0603360.
- [85] J. Navarro, private communication